Joint mAster of Mediterranean Initiatives on renewabLe and sustainAble energy

Deanship of Graduate Studies, Al-Quds University

"Development of a prototype of a sustainable magnetocaloric cooling device"

Fatima Muhammed Husain Battat

MS Thesis

Jerusalem - Palestine

1443/2022

Deanship of Graduate Studies, Al-Quds University

"Development of a prototype of a sustainable magnetocaloric cooling device"

Fatima Muhammed Husain Battat

A thesis submitted in partial fulfillment of requirement for the degree of Masterof renewable energy and sustainability

Supervisors

Dr. Husain Alsamamra
Physics Department, Al-Quds University, Palestine

Prof. Karen Friese
Jülich Center for Neutron Science-2, Forschungszentrum Jülich, Germany

Jerusalem - Palestine
1443/2022

Deanship of Graduate Studies, Al-Quds University

Thesis Approval

"Development of a Prototype of a Sustainable Magneto-Caloric Cooling Device"

Fatima Mohammed Husain Battat
Registration No: 21811715

Supervisors
Dr. Husain Alsamamra, Physics Department, Al-Quds University, Palestine.
Prof. Karen Friese, Jülich Center for Neutron Science-2, FZ Jülich, Germany.

Master thesis submitted and accepted, Date: 26.3.2022

The names and signatures of the examining committee members are as follows:

1- Head of Committee: Dr. Husain Alsamamra Signature 

2- Internal Examiner: Dr. Hazem Doufesh Signature 

3- External Examiner: Dr. Karam Awawdeh Signature 

Jerusalem - Palestine

1443/2022

Dedication

I am dedicating this thesis to two beloved people who have meant and continue to mean so much to me. Although they are no longer of this world, their memories continue to regulate my life. First and foremost, to my **MOM (Hamda)** whose love for me knew no bounds and who taught me the meaning of life and the value of hard work. I will make sure your memory lives on as long as I shall live. I love you and miss you beyond words. May Allah grant you Jannah.

Next, my little angel **"Israa"** whose life was cut short by a doctor's mistake at 18 years old. May you find peace and happiness in Paradise!.

To my beloved sisters **Hasna, Siham, Bahiya**, and my nieces **Iman**, and **Yasmin**, who bore my concern a lot. To my brothers', and friends, for supporting me all the way.

And everyone who believed in me encouraged me and gave me love to continue this journey.

Declaration

I certify that this thesis submitted for the degree of the master is the result of my research, except where otherwise acknowledged, and that this thesis, neither in whole nor in part, has been previously submitted for any degree to any other university or institution.

The work* was done under the supervision of Dr. Husain Alsamamra from the physics department-Al-Quds University.

Name: Fatima Battat

Signed: 

Date: 19 / 4 / 2022

Acknowledgments

I am thankful to **Dr. Husain Alsamamra**, for his guidance, support with full encouragement, my deepest thanks for allowing me to compete for this scholarship. I would like to express my deepest gratitude to my supervisor, **Prof. Karen Friese**, whose sincerity and encouragement I will never forget. This thesis would not have been possible without her, whose guidance from the initial step in this work enabled me to develop an understanding of the subject, she is the true definition of a leader and the ultimate role model. It is an honor to be one of her team.

I would like to acknowledge **Dr. Jörg Voigt** the head of instrument technology, who has been such a wonderful pairing with Dr. Karen for guiding me in the right direction to get this workout. Very special thanks to my great teammates, the technical staff from the Julich Center for Neutron Science (JCNS-2), **Micha Hölzle**, the technician for mechanical engineering, **Klaus Bussmann**, electronics engineer, and **Andreas Möller**, electronics engineer, I am thankful for the extraordinary experiences they arranged for me and for providing opportunities for me to grow professionally in different things.

I would also like to thank **Dr. Helmut Soltner**, an expert on magnetism and magnetic devices, from Central Institute for Engineering Electronics and Analytics, Engineering and Technology (ZEA-1), who provided me his valuable suggestion in magnet construction and simulation. I am grateful for my family sisters, brothers, nephews, and nieces whose constant love and support keep me motivated and confident. My success and accomplishments are because they believed in me.

My deepest thanks to the wonderful smiley faces in JCNS2, **Prof. Thomas Brückel, Dr. Asma Qdemat, Dr. Mai, and Miss Barbara Daegener**, Your smiles gave me positive energy, Big thanks to the German Palestinian Science Bridge (GPSB), for giving me this scholarship.

My heartfelt thanks to my estranged friends **Amal**, **Deema,** and **Nour'** who are always supportive of my adventures. I owe my deepest gratitude to them. I am eternally grateful for the love and support throughout the entire thesis process and every single day in Germany.

Fatima Battat

Abstract

Magnetic Refrigeration (MR) is a new cooling technology using a solid refrigerant instead of a gaseous refrigerant used in conventional cooling technics. The solid refrigerant is magnetocaloric material (MCM), its temperature increases when exposed to an external magnetic field causing magnetization of MCM, and the demagnetization happens to MCM by removing the external magnetic field which decreases the temperature of MCM. The magnetocaloric effect (MCE) is the phenomenon that describes the change of temperature of an MCM which is considered the basis of magnetocaloric refrigeration technologies. Compared to the conventional vapor compression cycle, the magnetocaloric cooling cycle is more energy-efficient and more environmentally friendly because it does not make use of greenhouse gases.

In this thesis, we develop a prototype of a sustainable magnetocaloric cooling device. A suitable design for the prototype was chosen and performed using the Autodesk inventor professional 2021 3D design program.

The components of our magnetic refrigeration device were selected and divided into four sub-systems: Magnetic Field Generator (MFG) consisting of the magnet and its mechanism, Active Magnetic Regenerator (AMR) containing the Magneto-Caloric Material, Fluid flow/heat transfer system, and the Control system.

An initial magnetic field generator was selected, which consists of two concentric 90 mm long Halbach cylinders, made of 16 permanent magnet segments, which were integrated with a support structure in optimized orientation, the outer cylinder is fixed and the inner one rotates with respect to the outer one producing two areas of maximum (1.3 T) and minimum (0.0002 T) magnet flux densities used to magnetize and demagnetizing the MCM to produce the cooling cycle.

The greatest effort expended in this master's thesis was to design an MFG at a low price. Various designs of the MFG were implemented on Autodesk inventor and simulated on Faraday simulation software. We decrease the number of segments to half (8 segments) and replaced the other 8 with soft magnetic low-carbon steel. The simulation results showed that the new design can generate a 0.8 T magnetic field, and thus the price of the magnet was halved, but its price remained very expensive we were limited by budget money.

Magnetic Arrangement for Novel Discrete Halbach Layout (Mandhalas) consisting of the final MFG. The final Mandhalas MFG produced a magnetic field of 0.82 T at the center of the magnet fined by simulation results and 0.6 T calculated by equations.

The support structure for the magnet circuit was designed with the program Autodesk inventor and the components were subsequently manufactured at the JCNS2 workshop. The housing was designed for the final mandhala magnet by the Autodesk Inverter program, then these designs were printed at the JCNS2 Institute, and the strong magnets were purchased and arranged in a certain way according to the simulation results. The Mandhala produced a magnetic field of 0.6 T at the center of the magnet measured by the axial Hall probe and transverse flowmeter.

The magnet design was improved and developed, as we were able to reduce the price of the magnet by 90%, while the decrease in the magnetic field of the magnet circuit was 36%.

The AMR was selected by choosing the type and the geometry of the MCM used to place into the inner magnet cylinder. We used Calorivac material from Vacuumschmelze company. A mixture of 80% water and 20% ethylene glycol is used as heat transfer fluid.

The control system was planned and relies on individual components which are easily accessible and are already available. The fluid flow/heat transfer system was also designed and the components were ordered.

Table of Contents

List of Figures

List of Tables

List of Abbreviations

MR	Magnetic Refrigeration
HCCs	Hydro-Chloro-Carbons
HCFCs	Hydro-ChloroFluoroCarbons
CFCs	ChloroFluoroCarbons
MCM	Magneto-Caloric Material
MCE	Magneto Caloric Effect
AMR	Active Magnetic Regenerator
HTF	Heat Transfer Fluid
Nd-Fe-B	Neodymium, Iron, Boron
ΔT_{ad}	Adiabatic Temperature Change.
S_M	
S_{ele}	Electric Entropy
S_{lat}	Lattice Entropy
MFG	Magnetic Field Generator
Mandhalas	Magnetic Arrangement for Novel Discrete Halbach Layout

Chapter 1

1. Introduction

1.1.1. Motivation:

Magnetic refrigeration at room temperature has been considered a competing alternative to the traditional cooling technology[**1**]. The traditional vapor-compression refrigeration devices use a compressor for compressing refrigerants, which absorb and release heat when compressed or decompressed [**2, 3**]. The refrigerants that were commonly used in vapor compressions systems such as hydro-chlorofluorocarbons (HCFCs), chlorofluorocarbons (CFCs), and hazardous chemicals (ammonia), were already banned some time ago because they are related to ozone depletion and global warming. HCFCs and CFCs have therefore been replaced by hydrofluorocarbons (HFCs). However, HFCs are now considered one of the main perpetrators of the greenhouse effect, so they will be prohibited soon according to the Montreal Protocol [**4**].

These compounds are harmful to the environment as they are ozone-depleting or greenhouse gases and thus contribute to the increase in global warming [**3**].

Cooling applications represent about 17% of the overall electricity consumption[**3**], which equates to 300 TWh. It is predicted that the demand will increase to 10,000 TWh in the year 2100 [**3**].

Conventional refrigeration is a well-established technology for more than 100 years [**3**], but in the past two decades, a great interest has emerged in alternative technologies based on magnetic refrigeration. This interest is directly linked to recent achievements in materials science and the development of new technologies that make it realistic to obtain solid refrigerators that make use of magnetic refrigeration [**5**].

Magnetic refrigeration depends mainly on the magneto-caloric effect (MCE), that is the change in the temperature of magnetic material when subjected to a change in the magnetic field. The MCE was discovered by Warburg in 1880 [**3, 6, 4**].

The magnetocaloric cooling cycle is based on magnetizing and demagnetizing a solid refrigerant and is largely analogous to the vapor-compression cycle used in conventional refrigerators [**7**].

Magnetocaloric cooling technologies have several benefits, e.g. the absence of a vapor refrigerant that is harmful to the environment [**6**], the provision of more comfortable and environmentally friendly living conditions [**3**], as well as the absence of a compressor and thus a more silent cooling device [**7**]. It has been shown that magnetic refrigerators operating with gadolinium (Gd) as a refrigerant have a high efficiency that reaches up to 60% of the Carnot cycle system, whereas in the conventional refrigerator the Carnot efficiency is only 40%. This means that magnetic refrigeration could save up to 20% in energy when compared to the vapor-compressor refrigerator [**4**].

1.1.2. Place of work

This master's thesis was completed in Germany at the Jülich Research Center, specifically at the Institute of Jülich Centre for Neutron Science (JCNS-2; figure 1), and with an integrated work of a team consisting of the supervisor Prof. Karen Friese (deputy institute director) and Dr. Jörg Voigt, head of instrument technology. The team is completed by technical staff from the JCNS-2: Micha Hölzle (technician for mechanical engineering and institute responsible for IT services), Klaus Bussmann (electronics engineer and health and safety representative), Andreas Möller (electronics engineer) from the instrument technology at JCNS, Dr. Helmut Soltner (expert on magnetism and magnetic devices) from Central Institute for Engineering Electronics and Analytics, Engineering and Technology (ZEA-1), and me.

Figure 1.1: Jülich Center for Neutron Science (JCNS)

1.2. The general theory of refrigeration system

Refrigeration is defined as lowering the temperature of an enclosed space by removing heat from that space and transferring it to another place. This function is performed e.g. by a refrigerator.

The basic refrigeration cycle depends on the laws of thermodynamics. Energy can be stored within systems in different forms: kinetic energy, potential energy, and internal energy [**8**]. The different forms of energy can be transformed from one form to another, and transferred between systems, by work and heat transfer. The first law of thermodynamics states that, in closed systems, the total amount of energy is conserved in all transformations. The second law of thermodynamics states that the sum of the entropies of the interacting systems never decreases[**8**]. It also states that heat always flows from a material at a high temperature to a material at a low temperature.

1.3. The principle work of the Magnetic Refrigeration System

The development of MR started when the German physicist Emil Warburg discovered the magneto-caloric effect (MCE) in iron in 1881 [**3, 6**], yet the use of the MR at room temperature was practically made possible much later with the discovery of magneto-caloric

materials (MCMs), such as Gadolinium (Gd) and its alloys, which show the MCE at room temperature [**9**].

1.3.1. Magneto-Caloric Effect (MCE):

The MCE describes the change of temperature of a material when exposed to a changing external magnetic field under adiabatic conditions. Materials exhibiting this effect are called magneto-caloric materials (MCMs)[**10**].

The MCE can be described by the isothermal magnetic entropy change (ΔS_m), or the adiabatic temperature change (ΔT_{ad}) of the MCM, induced by increasing or decreasing an external magnetic field that the material is subjected to [**11**].

1.3.2. Magnetic Refrigeration Cycle:

The magnetic refrigeration cycle is shown in figure 1.2 and figure 1.3, it consists of the following steps:

(i) Adiabatic magnetization: by increasing adiabatically the magnetic field (+H) applied on a magneto-caloric material (MCM) at temperature (T), the total entropy of the magnetic solid matrix remains constant. However, the decrease of the magnetic entropy due to the magnetic field variation is compensated by an increase in the lattice and electronic entropy contributions, forcing the magnetic spins to align. As a consequence the temperature of the material increases to ($T+\Delta T_{ad}$), (figure 1.3). [**8**] [**12**].

(ii) Keeping the applied magnetic field constant, a heat transfer fluid (HTF) is then circulated from CHEX through the regenerator (MCM). The HTF absorbs heat from the MCM, which cools down the MCM and releases heat to the fluid, and rejects heat to a hot source (ambient) at HHEX [**12, 13**].

(iii) Adiabatic demagnetization: Keeping the refrigerant thermally insulated in the magnetized condition, the magnetic field is then switched off (-H). The magnetic

spins disorder and the temperature of the MCM decrease (T -ΔT_{ad}). This process is called adiabatic demagnetization [**13**].

(iv) Now the HTF is circulated on the MCM and gets cooled. The cooled fluid is then circulated to a device that is cooled down with it. This process corresponds to heat absorption (+Q). These four steps are repeated for continuous cooling [**13**].

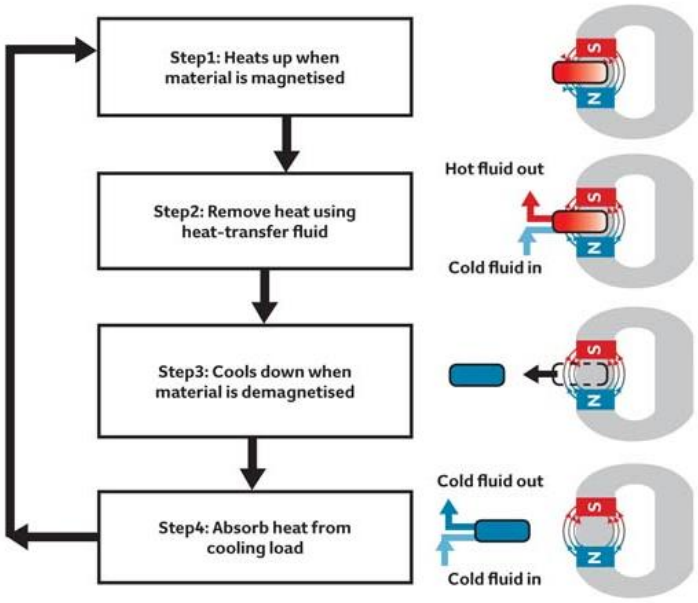

Figure 1.2: The basic working principle of magnetic refrigeration (MR) [14].

1.4. Comparison between conventional and magnetic refrigeration:

The magnetic refrigeration cycle is analogous to the conventional vapor compression cycle. A comparison between the two cooling cycles is explained in the following points (figure 1.3).

- The magneto-caloric refrigeration requires the input of energy to magnetize the magneto-caloric material (MCM), which acts as a solid refrigerant, while vapor-compression refrigeration requires mechanical energy to compress the vapor refrigerant.

- In an MR cycle, the solid refrigerant is magnetized which then leads to an increase in its temperature. In the vapor compression cycle, the vapor refrigerant is compressed, which leads to an increase in temperature.

❖ The demagnetization decreases the temperature of the MCM material, while in the vapor compression cycle the expansion process leads to a cooling down of the vapor refrigerant. [**15**].

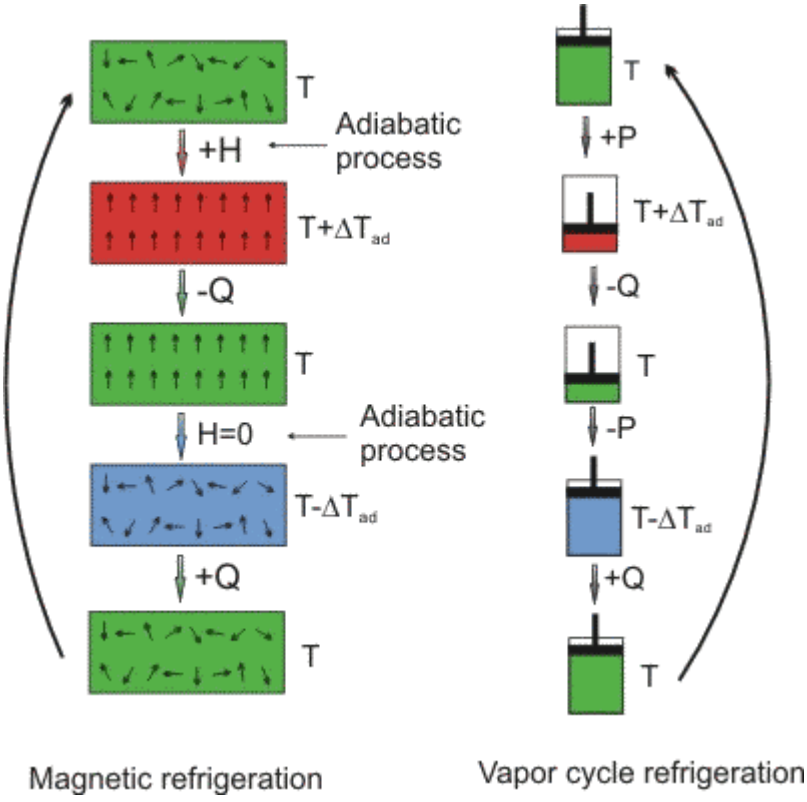

Figure 1.3: Magnetic refrigeration Vs. conventional vapor compression refrigeration cycles [16].

Chapter one explained magnetic refrigeration. A comparison was made between magnetic refrigeration and traditional refrigeration. In chapter two, we will talk about MR theory and display some prototypes of magnetic refrigeration that were built in previous years that were discussed in the literature of MR. In chapter three, the methodology and results of the work carried out in this research will be clarified, which broadly and accurately presents the process of designing, developing, and building the magnetic field generator at the lowest possible price. In chapter four, the conclusions of the thesis, and the future work were presented.

Chapter 2

2. Magnetic Refrigeration Theory and Literature review of magnetic refrigeration

This chapter discusses the theory of magnetic refrigeration and how the magnetocaloric effect (MCE) can be measured directly and indirectly. The history of magnetic refrigeration was also discussed and presented some prototypes that show how magnetic refrigeration has evolved from its appearance to the present time.

2.1. Thermodynamics of Magneto-caloric Effect (MCE)

The MCE is described by the isothermal entropy change (ΔS_m), or the adiabatic temperature change (ΔT_{ad}) of the MCM, induced by increasing or decreasing the external magnetic field strength (H). It is defined in equations (2.1) and (2.2) and graphically illustrated in Figure 2.1 [**13**].

$$\Delta S_m(T, H_f, H_i) = S_f(T, H_f) - S_i(T, H_i) \quad (2.1)$$

$$\Delta T_{ad}(S, H_f, H_i) = T_f(S, H_f) - T_i(S, H_i) \quad (2.2)$$

Where H_f and $H_i$are the final and initial magnetic fields, S_m is the magnetic entropy [**17**].

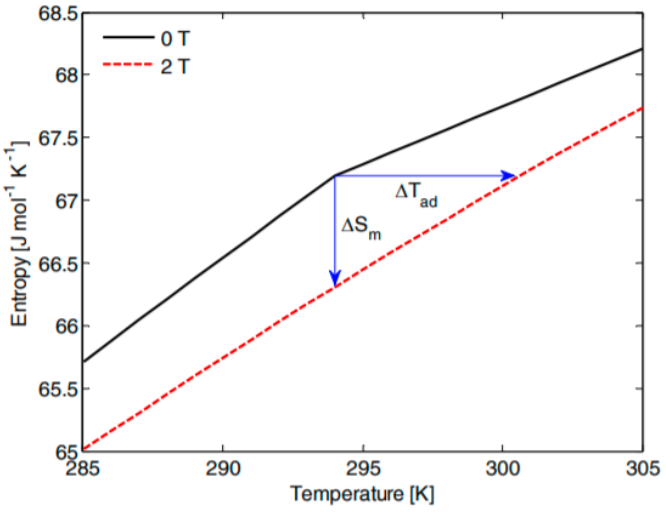

Figure 2.1: The S-T diagram represents the existence of the MCE [**13**].

The direct way to characterize the MCE is by measuring the temperatures (T_i & T_f) by using a temperature sensor in thermal contact with the MCM. This yields the adiabatic temperature change ΔT_{ad} [**18**].

The indirect way for characterizing the MCE is by determining the magnetic entropy change ΔS_m.

The total entropy in a system consists of magnetic entropy (S_M), lattice entropy (S_{lat}), and electric entropy (S_{ele}):

$$S = S_M + S_{lat} + S_{ele} \tag{2.3}$$

In an adiabatic system, the magnetic entropy S_M is a function of temperature and magnetic field strength s(T, H). At constant volume and pressure, the differential change in entropy can be written as [**17**]:

$$dS_M = \left(\frac{\partial s}{\partial T}\right)_H dT + \left(\frac{\partial s}{\partial H}\right)_T dH \tag{2.4}$$

Where, (s) is the specefic entropy.

By using the definition of the specific heat (at a constant field) $C_H = T\frac{\partial s}{\partial T}$, equation (2.4) can be rewritten as [**17**] :

$$ds(T,H) = \frac{C_H(T,H)}{T} dT + \left(\frac{\partial s}{\partial H}\right)_T dH \tag{2.5}$$

If the magnetic field is changed adiabatically, the temperature change is [**17**]:

$$dT = -\frac{T}{c_H(T,H)}\left(\frac{\partial s}{\partial H}\right)_T dH \tag{2.6}$$

By integrating from the initial to the final magnetic field (H_i and H_f), one obtains the adiabatic temperature change as follows [**17, 19**]:

$$\Delta T_{ad} = -\int_{H_i}^{H_f} \frac{T}{c_H(T,H)}\left(\frac{\partial s}{\partial H}\right)_T dH \tag{2.7}$$

And by using Maxwell's relations for the equivalence of the second derivatives of (2.6) [**17**]:

$$dT = -\frac{T}{c_H(T,H)}\left(\frac{\partial M(T,H)}{\partial T}\right)_H dH \quad (2.8)$$

Finally, MCE can obtain from equation (2.9) [**17, 19**]:

$$\mathbf{MCE} = \Delta \mathbf{T_{ad}}\,(\mathbf{T}, \Delta \mathbf{H}) = -\int_{\mathbf{H_i}}^{\mathbf{H_f}} \frac{\mathbf{T}}{\mathbf{c_H(T,H)}}\left(\frac{\partial \mathbf{m(T,H)}}{\partial \mathbf{T}}\right)_{\mathbf{H}} \mathbf{dH} \quad (2.9)$$

Where, $\Delta H = H_f - H_i$.

2.2. Literature review of magnetic refrigeration and the most common devices :

The first step in magnetic refrigeration (MR), was taken by Warburg, who discovered the MCE in iron in the **1880s** [**5**]. Then in **1890**, Tesla tried to run a heat engine depending on this effect, later; the low sub-Kelvin temperature was obtained by proposed MR in low-temperature physics by Debye and Giauque [**20**]. MR took a quantum leap in **1976** when NASA built the first magnetic heat pump working at room temperature [**20, 21, 22, 23, 24**]. This prototype is shown in figure 2.2

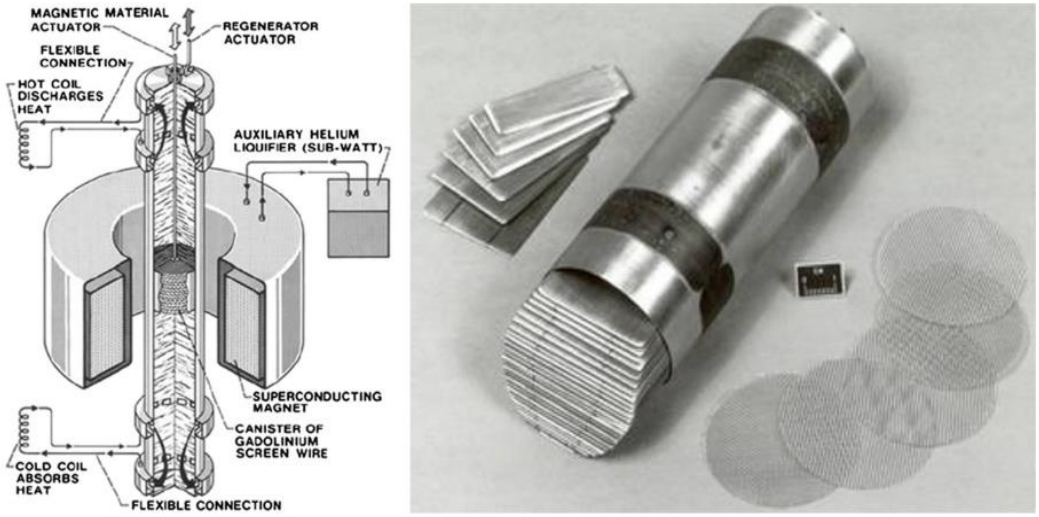

Figure2.2: The first room-temperature magnetic heat pump was designed by Brown in 1976 [22].

Brown had obtained a breakthrough by building this heat pump, it contained a superconducting magnet, cooled by liquid helium, and produced a 7 T magnetic field. It covered a temperature range of 47 K. The principle of operation of Brown's machine was based on the linear movement of the magneto-caloric material (MCM) through the magnetic field. The magnetic material was a stack filled with 1 mm thickness parallel plates of

gadolinium (Gd). The heat transfer fluid (HTF) used was a mixture of 20% ethyl alcohol with 80 % of water mixture [**21**]. The maximum temperature span was 80 K (from 248 to 328 K). The frequency of operation was low, which caused low efficiency and cooling power [**22**].

After 1976, many scientific inputs occurred into the field of magneto-caloric energy conversion near room temperature. Over the past 45 years, a large number of different prototypes have been designed and built [**21**].

In 1998, Zimm et al. built and presented a reciprocating device, shown in figure 2.3, by Astronautics Technology Center and Ames Laboratory from Iowa State University [**21**].

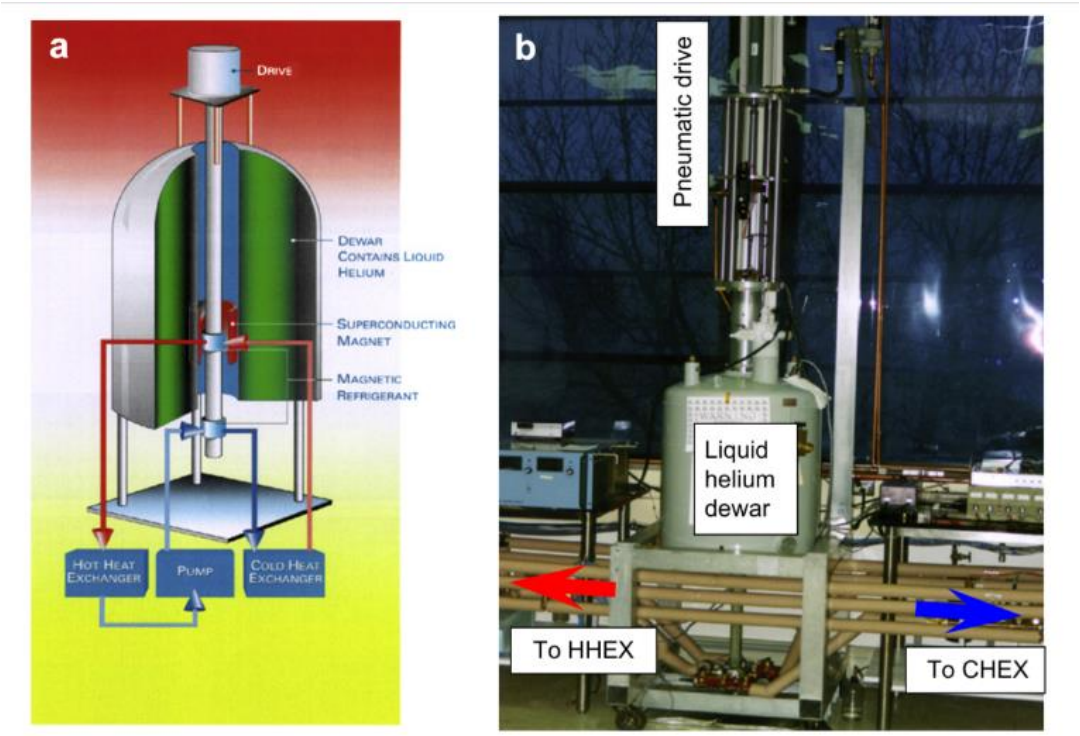

Figure 2.3: Prototype built by Astronautics Technology Center and Ames Laboratory in 1998: (a) schematic and (b) photograph [**25**].

This prototype consisted of fixed Niobium–titanium (Nb−Ti) superconducting magnets, and two active magnetic regenerators (AMRs), moving reciprocally in and out of this magnet. Each AMR contained 1.5 kg of Gd spherical particles with a diameter varying between 0.15 and 0.3 mm, and the produced magnetic field was 5 T, using water as HTF. This device produced a cooling power of 200 W kg−1 for a temperature span of 9 K at 5 T magnetic field, and 70 W kg−1 cooling power at 7 K and 1.5 T [**21, 25**].

Great attention had been attracted to magnetic refrigeration in recent years. In the beginning, the magnetic prototypes used superconducting magnets to obtain high magnetic flux densities in the MCM, but later; most prototypes obtained magnetic flux densities from permanent magnets [**20**], in order to take advantage of their energy efficiency and spatial compactness [**1**].

In **2007**, Buchelnikov, V. D., et al. built a rotary prototype shown in figure 2.4, which consists of a fixed permanent magnet that acted as a source of 1 T magnetic field, and a rotary magnetic refrigerant made of Gd, This prototype was presented by the Chelyabinsk State University, it produced 40 W cooling power, by using 0.6 – 1.5 l/min flow rate of the heat transfer fluid, at an operation frequency of 1-10 Hz [**22**].

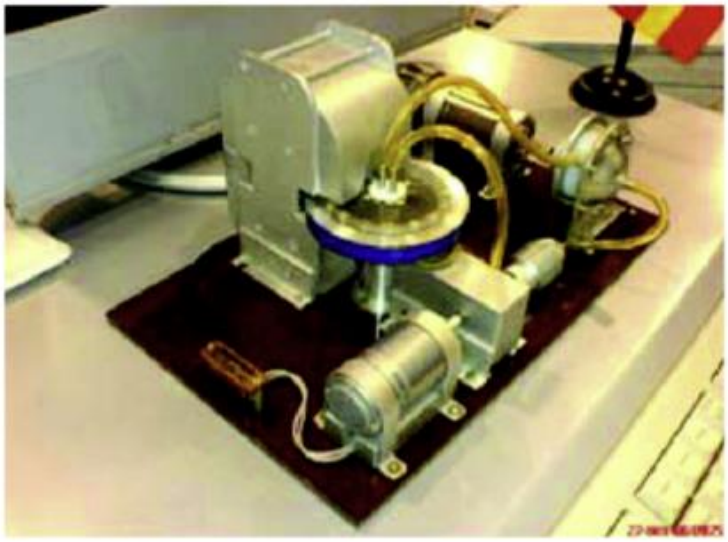

Figure. 2.4: Rotary magnetic refrigerator, presented by the Chelyabinsk State University, in 2007 [**22**]

A slow increase in the number of prototypes built at the beginning, but suddenly, the interest of scientists increased significantly in studying this technology. They began competing to produce a commercial product. **6** devices were built in **2007**, then **11** different MC refrigerator units had been built and designed in **2009**, it had been built in Japan, China, Brazil, 2 devices in France, Korea, Denmark, Switzerland, Italy, Canada, and Slovenia [22].

In **2010**, Yu, B., et al. presented in detail **41** devices and operation principles, which had been built before 2010. Yu, B., et al. confirmed that the efficiency of these devices that were built

during that period was still low, because of pressure losses by the HTF, which is too significant to achieve a high refrigeration performance. However, efficiency improvements of 20% - 30% compared to traditional refrigerators today [**22**].

In **2015**, Kitanovski, A., et al. posted an overview of existing magnetocaloric (MC) prototype devices before the year 2015 [**23**]. The same team had written a book in **2016**, about MC energy conversion, which includes a detailed explanation of all these devices [**21**].

Kitanovski, A., et al. confirmed that magnetic refrigeration was on the brink of commercialization in that period, and there was a slow improvement achieved with every new prototype that had been built, but these improvements were measurable toward the magnetic refrigeration goal. The number of prototypes increased every year, according to expanding research activities in the magnetocaloric (MC) energy conversion research community, but several obstacles needed to be overcome before finalizing the idea of commercializing MC technology. Prototypes in this period had been divided into two groups; according to the motion of the magnet source and AMR, reciprocating motion, and rotation motion [**23**].

Kitanovski, A., et al. introduced **29** devices of reciprocating motion prototypes, the operating frequencies in these devices were limited to 1 Hz and below, which affects the specific cooling power, those devices were mostly used as AMR testing devices. They were designed in such a manner that different AMRs can be easily interchangeable, the first one was Brown's device [**21, 23**].

The other group of prototypes was operating in a rotary motion, Kitanovski, A., et al. described in detail **32** different rotary devices, those prototypes focusing on the AMR and magnet assembly design, also on the fluid-flow circuits, valve systems, heat exchangers, the choice of the MC material geometry and driving system for rotating the AMR/magnets, because; all of these components affected the efficiency of the device. But these devices still need a lot of optimization and development [**21**].

in 2018, the first MC prototype used recycled Nd–Fe–B permanent magnets, shown in figure 2.5, and a La–Fe–Mn–Si for the MC heat exchanger, as a Gd replacement material [**3, 24, 26**].

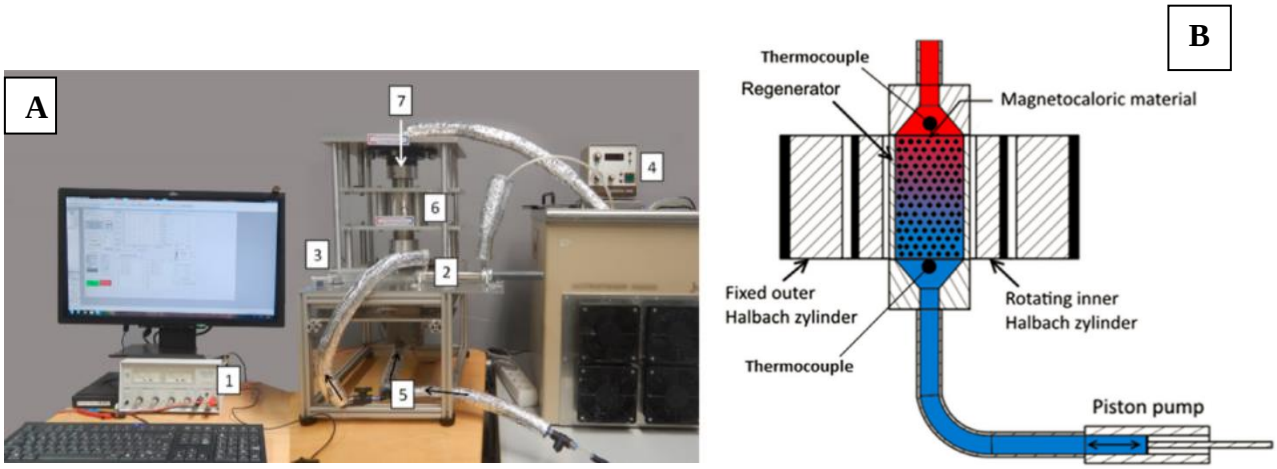

Figure 2.5: The first MC prototype used recycled Nd–Fe–B permanent magnets, source [**3**]

A: Photograph, B: Magnetocaloric demonstrator with components: 1) Power supply 2) fluid pump; 3) setting for phase difference; 4) water reservoir with heating and cooling conditioner; 5) water hoses pipes; 6) recycled Halbach-magnet; 7) regenerator insert., B: Schematic

In **2019**, Greco, A., et al. published a review about solid-state prototypes used as cooling and heat pumps, developed before the year 2019 [**24**]. Greco, A., et al. focused on prototypes built between 2015 and 2019, where they discussed in detail almost **11** prototypes that adopt MCE in refrigeration technology [**24**]. With the increasing energy demand, research had been increased in cooling technology, so by focusing on magnetic field generators, side by side with the search for materials with high MCE. In this period, most MR devices used permanent magnets. These magnets developed from the simple (C) shaped, into a complicated concentric Halbach cylinder [**1**].

A lot of steps were taken in MC prototype development, so we had devices that can produce cooling powers up to 3042 W and temperature spans around 40 K [**24**].

Niamjan, N., et al. **in 2020**, modified the magnetic flux distribution in the Halbach cylinder, by inserting a soft magnetic rod in the core of the magnet cylinder, also presented the effect of substitution of some permanent magnet segments in a Halbach cylinder with soft magnetic materials, which reduces the cost in the real structure but it decreased the flux density in the air gap [**27**].

Many studies and experiments had been done in the field of materials science, for the processing of MCMs, focusing on the development of efficient and rapid heat transfer methods. **In 2020**, He, J., et al. presented a comparative study on the series, parallel, and cascade cycles of a multi-mode room temperature MR system. They were comparing the refrigeration characteristics of three modes, the MCM used is 277.4 g of gadolinium, and two Nd-Fe-B permanent magnets provide 1.5 T maximum magnetic field intensity. The results provide some guidelines for designing MR prototypes [**28**].

Also **in 2020**, He, J., et al., presented 'active magneto-caloric heat pipe shown in figure 2.6.

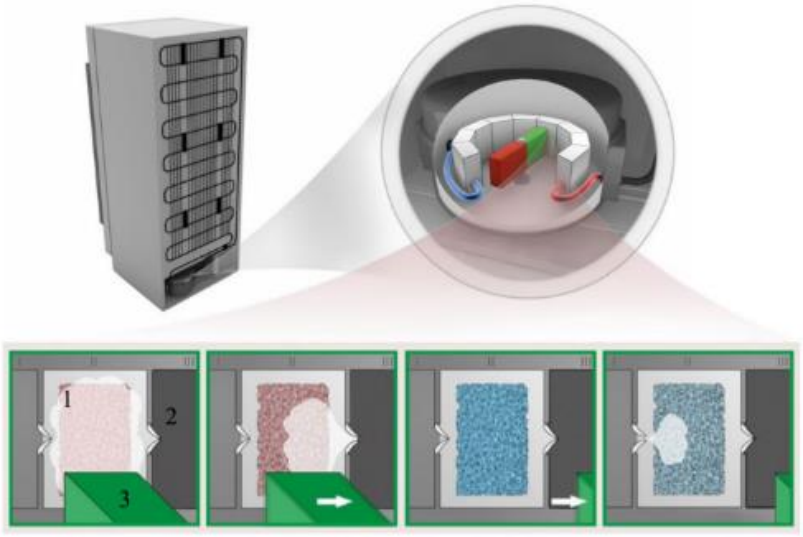

Figure 2.6: Schematic structure of the active MC heat pipe. (1) MCM, (2) check valve, (3) the magnetic field [**29**].

A single segment described in figure 2.6, consists of a sphere of $La(Fe-Mn-Si)_{13}$ with a diameter of 200–400μm, like 3.5g MCM, and a 1.2 T magnet system, with a peak temperature of 20.7°C. Methanol acts as a heat transfer fluid (HTF), two check valves, an evaporator wrapped with heating wire insulated thermally to the environment, and a condenser connected to a thermal bath at an adjustable temperature. This system detected a maximum specific cooling power of 12.5W/g at a frequency of 20 HZ [**29**].

Until the moment of writing this thesis, many kinds of research written and prototypes build, to improve the performance of magnetic refrigeration (MR). These works focus on the most critical two parts of MR, the first one is the magnetic field generator (MFG), The second critical part is the active magnetic regenerator (AMR).

any small change in the components of the MR system, specifically the MFG and AMR leads to a change in the whole system, and therefore scientists and researchers are still trying finalizing the idea of commercializing MC technology, used to transition from conventional cooling to MR.

What we seek to develop in this master thesis, is to collect all that was recommended in previous research in one prototype. We want to start where others ended. The magnetic field generator (MFG) is made of permanent magnets recommended according to the latest research. A rotary motion prototype. Two concentric Halbach cylinders as MFG. Building an MFG at the lowest possible price. All these points meet together in some previously built MC prototypes, but the MFG is always very expensive, so we will combine all these points in building an MR prototype with a very low magnet price.

Chapter 3

3. Development and Improvement of our Magneto-Caloric cooling prototype.

In this chapter, the practical part of building the magnetocaloric cooling prototype was described, the initial designs that were implemented, and how they were improved and developed until we reached the final design in detail.

3.1. Choice of the basic design

In magnetic refrigeration, to obtain a complete cooling cycle, any prototype must consist of four integrated sub-systems, that work together to complete this cycle. As shown in figure 3.1, these main sub-systems are; the Magnetic Field Generator (MFG), Active Magnetic Regenerator (AMR), which consists of Magneto-Caloric Material (MCM), Fluid Flow/Heat Transfer System, inside this system the Heat Transfer Fluid (HTF) circulates, and the Control System that controls and synchronizes all these systems together.

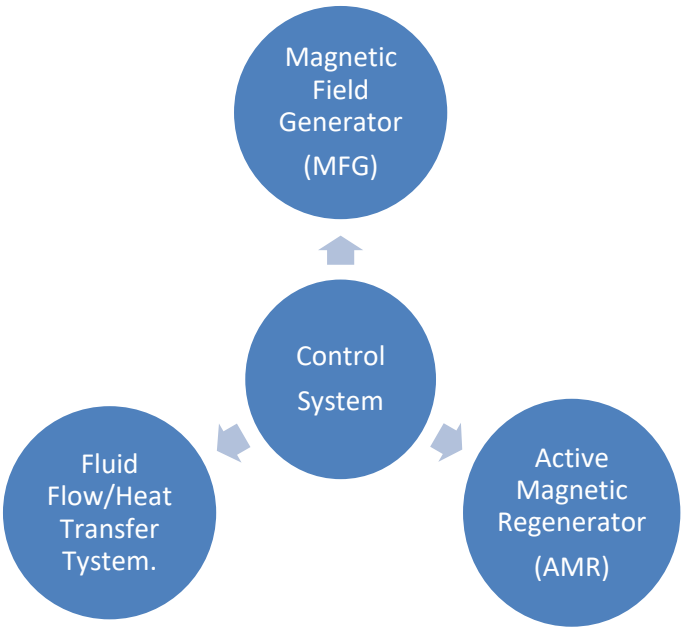

Figure 3.1: Main four sub- systems of Magneto-Caloric cooling

The methodology of building our magnetic refrigerator prototype consisted of the following steps, which are described briefly in figure 3.2

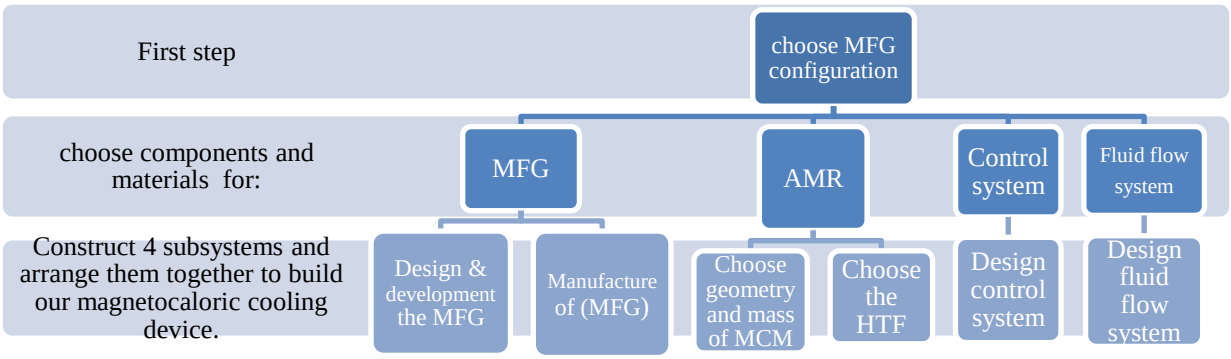

Figure 3.2: Flowchart describes the steps of building our magnetic cooling prototype.

Due to the closures resulting from the Corona pandemic and the disruption of the work of some factories and institutions in Germany, there was a delay in building the prototype. The greatest effort that has been made in this master's thesis is to develop, improve and construct the magnetic field generator (MFG).

3.2. The main components of the introduced Rotary Magneto-caloric Cooling Prototype

The most important components of the final rotary magneto-caloric cooling prototype are illustrated in Figure 3.3. And table 3.1 summarizes the specifications of the prototype.

Table 3.1: The specifications of the introduced magneto-caloric cooling prototype.

Property	Range	units
Magnetic Field	0.0002- 0.6	T
Operating frequency	5	Hz
Heat Transfer Fluid	water-glycol mixture (80 % water, 20 % glycol)	
Regenerator Volume	55.3	cm^3
Regenerator Diameter	28	mm
Regenerator Length	90	mm

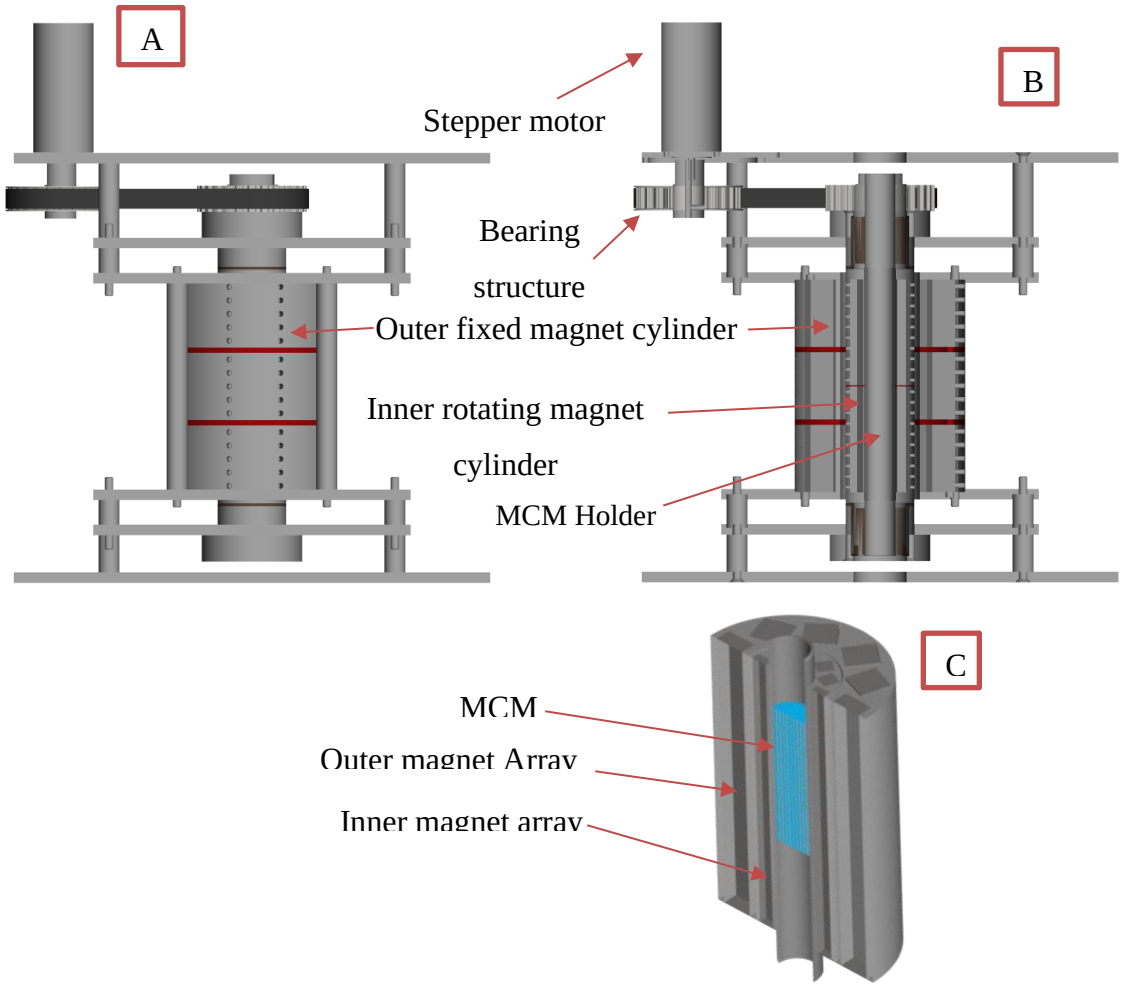

Figure 3.3: (A): The final design of the magnetocaloric cooling prototype, showing the bearing structure to enable the rotation of the internal magnet. **(B):** cross-section in the Y direction shows the magnetic circuit and AMR configuration,(**C**): closer look the magnet circuit housing showing the MCM at the core of the magnet circuit.

This final 3D design for our magnet field generator and the magneto-caloric material configuration, and the parts responsible for the movement mechanism to produce a continuous change of the magnetic field on the area that covers the MCM, is designed on the Autodesk inventor professional 2021 program.

Figure 3.3 shows the details of the drive system and the arrangement of the main components. The nested Mandhalas cylinders are installed vertically with the fixed outer magnet cylinder and the rotating inner magnet cylinder. The solid refrigerant (MCM) is accommodated in the magnet generator core. The system needs Pipes to transfer HTF between the hot and cold heat exchangers. The timing belt is used to drive the inner magnet relative to the outer magnet. Also, the system needs to measure the temperature change inside the heat exchangers using a

temperature sensor. Also, it needs a control system to synchronize the work of all these components.

The main motivation for this thesis is to improve the magnet design and reduce its price while maintaining its high performance, to generate the entropy change in the magnetocaloric refrigerant.

3.3. Designing the Magnetic Field Generator (MFG):

Researchers and scientists used different types of magnets to generate the magnetic field, but in recent years, the permanent magnets (PMs) were the greater majority used to build magnetic field generators. The PMs are preferred because they do not require power to generate a magnetic field [**30**].

As we mentioned before in the magnetic refrigeration cycle in chapter 1 section 1.3.2, in magnetic refrigeration systems we need to design a magnetic field generator to generate magnetic field profiles with regions of high and low magnetic flux density used to magnetize and demagnetize the MCM.

Different designs of permanent magnet configurations have been developed for magnetic refrigeration devices, the Nested Halbach cylinders configuration was used recently [**31**].

3.3.1. Nested Halbach cylinders configuration:

A Halbach magnet array is a specialized and interesting arrangement of permanent magnets, that was invented by Klaus Halbach in 1979 to increase the magnetic field on one side of the array while canceling it on the other side [**32, 33**]. Halbach arrays shown in Figure 3.4 can have linear, circular, or spherical geometry and generate dipolar or multipolar magnetic fields inside or outside the structure. The blue lines indicate the magnet flux. The magnetization directions are indicated by the red arrows located on a circle of radius r and at an angle θ while pointing at an angle α (see figure 3.4 (d)). This magnetization (M) is indicated in equation (3.1)[**33**]:

$$\mathrm{M}(\mathrm{R}, \theta) = M_0 \begin{pmatrix} \sin\alpha \\ \cos\alpha \end{pmatrix} \text{ with } \alpha = (1 + \mathrm{m})\,\theta \text{ and } \mathrm{m} \in \mathbb{Z} \qquad (3.1)$$

Where: M_0 is the magnetization at the center, m is the number of pole pairs, for example, m = ±1 for a dipolar, m = ±2 for a quadrupolar field, and the sign of m directs the flux either inwards (positive m) or outwards (negative m), $\mathbb{Z}$ is the set of integers [**33**].

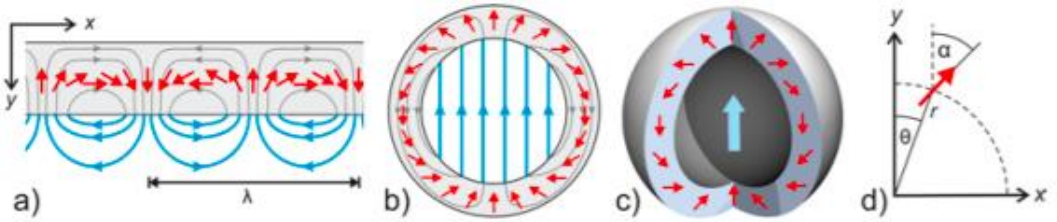

Figure 3.4: Schematic illustration of (a) linear, (b) cylindrical, and (c) spherical Halbach arrays. (d) Sketch of the coordinate system and the angles used for the construction of (b) and (c) [**33**].

The flux density inside the bore of an infinitely long Halbach cylinder is [**34**]:

$$\boldsymbol{B_{infin} = B_r \ln\left(\frac{r_o}{r_i}\right)} \tag{3.2}$$

Where B_r: is the magnitude of the remanent flux density of the permanent magnet used, r_i, r_o are the inner and outer radius of the magnet cylinders.

The flux density inside the bore of the finite length of the Halbach cylinder shown in figure 3.5 is given in equation (3.3) [31] :

$$\boldsymbol{B_{fin} = B_r\left(ln\frac{r_o}{r_i} + \frac{L}{4}\left(\frac{1}{\sqrt{\frac{L^2}{4}+r_i^2}} - \frac{1}{\sqrt{\frac{L^2}{4}+r_o^2}}\right) - ln\frac{\frac{1}{2}+\sqrt{\frac{L^2}{4}+r_o^2}}{\frac{1}{2}+\sqrt{\frac{L^2}{4}+r_i^2}}\right)} \tag{3.3}$$

Where L is the length of the Halbach cylinder.

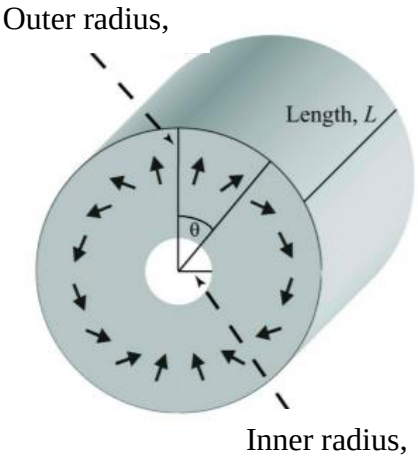

Figure 3.5: A sketch of a Halbach cylinder with an inner radius, r_{in} and outer radius, r_o, and length, L. Also, black arrows showed the direction of the magnetization of the magnetic material [34].

By dividing the Halbach cylinder into segments as shown in figure 3.6, each segment has its direction of magnetization with finite length. A Halbach cylinder with n segments has a magnetic flux density (B_{HC}) at its center given by equation (3.4) [**31**]:

$$\boldsymbol{B_{HC} = B_{fin}\left[\frac{sin(2\pi/n)}{(2\pi/n)}\right]} \quad (3.4)$$

Figure 3.4 shows the nested Halbach cylinders configuration which consists of two concentric Halbach cylinders so that each magnet array generates a magnetic field in its core, each finite length non-segmented Halbach cylinder generates a magnetic field density in its core equal to B_{fin} in equation (3.3) [**31**]. Halbach cylinders give a static magnetic field. In order to generate a variable field within the bore of the cylinder, we can nest two Halbach cylinders, and then control the magnetic field in the bore by changing the relative angle between the two cylinders [**35**].

The blue arrows in figure 3.6 indicate the remanent flux density of the permanent magnet segments, If the magnetic field contributions of each magnet are added, then the maximum magnetic flux density (B_{max}) of the NHC is observed at the core of the inner magnet, as shown in Figure 3.6 (A). Conversely, when the magnetic field contributions are subtracted, the minimum magnetic flux density (B_{min}) is obtained, as seen in figure 3.6 (B).

The maximum and minimum magnetic flux densities for the nested configuration are calculated by [31] :

$$B_{max} = B_{HC,O} + B_{HC,I} \quad (3.5)$$

$$B_{min} = |B_{HC,O} - B_{HC,I}| \quad (3.6)$$

, where $B_{HC,O}$: is the magnetic flux density of the outer magnet cylinder and $B_{HC,I}$: is the magnetic flux density of the inner cylinder.

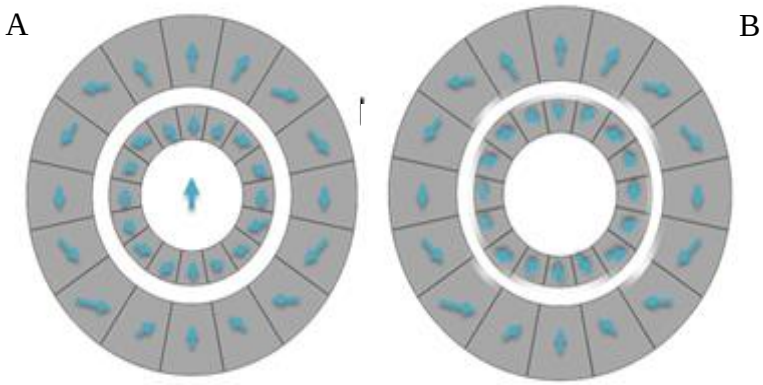

Figure 3.6: Nested Halbach cylinders magnet array: (A) The maximum magnetic field position (magnetization process) (B) The minimum magnetic field position (demagnetization process)

3.3.2. The Initial Design of the Presented Nested Halbach Magnet cylinder:

The initial magnet design, shown in figure 3.7, was designed by Autodesk inventor professional 2021 software, and the geometry dimensions are summarized in table 3.2.

Table3.2: Geometry of the initial magnet design

Cylinder	Inner Diameter (mm)	Outer Diameter (mm)	Length (mm)
Inner Halbach magnet	30	48.4	90
Outer Halbach magnet	58.4	96.6	90

This configuration consists of two concentric Halbach cylinders. Each magnet array consists of 16 permanent magnet segments. The dimensions of this magnet circuit have been chosen according to the restrictions discussed in the next section.

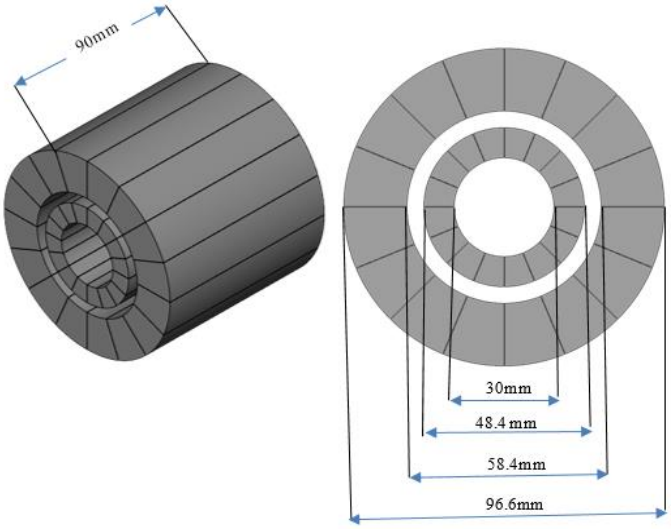

Figure 3.7: The initial design of our Nested Halbach magnet cylinder.

Figure 3.8 shows the initial design of the magnet housing circuit.

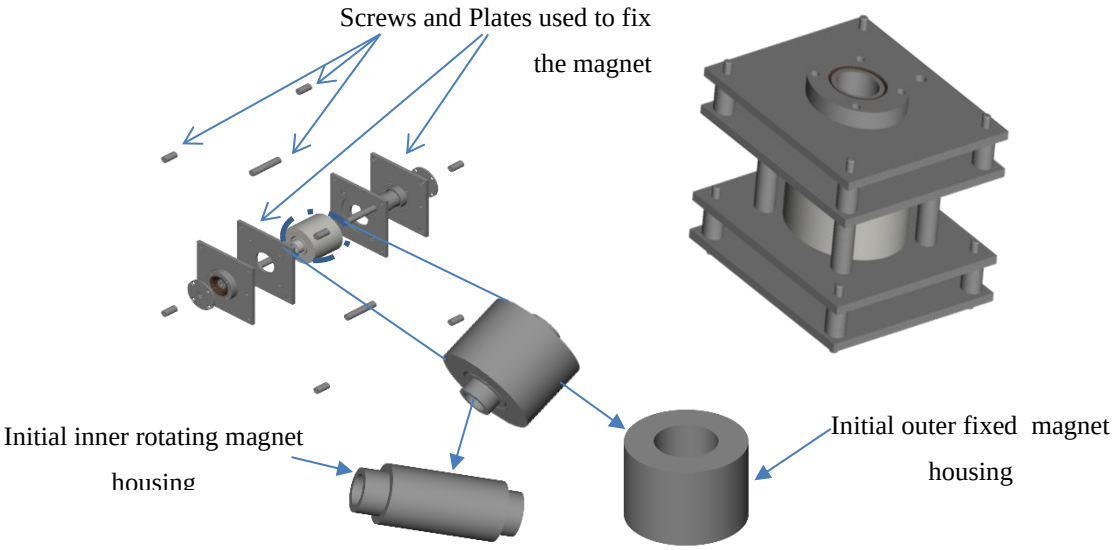

Figure 3.8: The housing design of the initial magnet.

3.3.3. Parameters and constraints in designing our magnet circuit:

We are restricted to the budget specified for the active magnet regenerator (AMR). Then the MFG is designed due to the regenerator dimensions. The inner diameter of the internal cylinder is directly related to the regenerator housing diameter. The air gap between the inner and outer magnet cylinders must be as small as possible, just to allow the inner magnet to rotate inside the outer cylinder without friction. The smaller the air gap the higher the magnetic field intensity at the nested Halbach cylinder core [**31**].

Since the magnet is the most expensive part of the magneto-caloric cooling device, the magnet price played an important role in choosing the final magnet design, which will be highlighted and discussed in the next sections.

3.3.4. The simulation results and discussion of the Initial magnet design (Nested Halbach):

The simulation results of the magnetic flux density profile for the initial magnet field generator are obtained at the center of the magnet by Faraday magnet simulating software, this result alternating from 1.4 T (maximum magnetic flux density) to 0 T (minimum magnet flux density) according to the rotating of the inner magnet cylinder **180°** with respect to the outer fixed magnet by **10°** every step, these results are shown in figure 3.9(A).

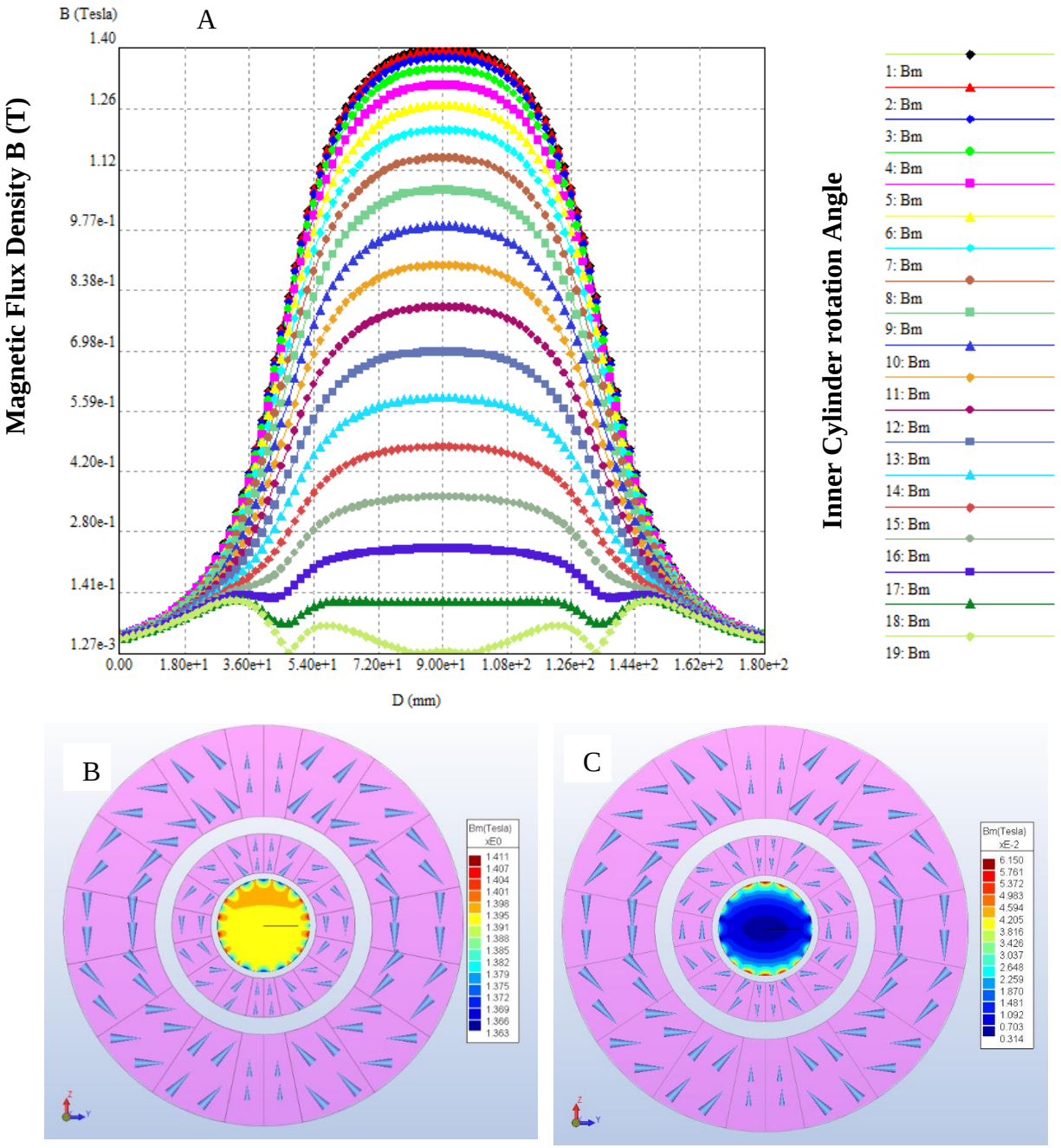

Figure 3.9: The simulation results of our initial nested Halbach magnet array using Faraday software, show the magnetic flux density at the cylinder core. The magnet length is 90 mm.

A: Magnetic flux density along the axial z-direction for different rotation angles **B:** Maximum magnetic flux density (magnetization) **C:** Minimum magnetic flux density (demagnetization).

Figure 3.9 (B and C) shows the maximum and minimum magnetic flux densities at the core of the magnet, which equals (**1.4 T and 0.003 T**), respectively. We obtained the maximum magnetic flux density when the magnetization directions of the two-cylinder magnets are

parallel (in the same directions), as shown in figure 3.6 (A). We obtained the minimum magnet flux density when the magnetization directions of the two magnet segments were in opposite directions (see figure 3.6(B)), Note that a different map is used for each magnet profile simulation.

Although this initial design can provide our cooling system with a **1.4 T** magnet flux density. But it is very expensive according to the manufacturing of magnet material and its magnetization. For this reason, we decided to search for other solutions to decrease the magnet price, according to our budget constraints.

3.4. Optimizing the Initial Halbach magnet design:

The following sections discussed the design development process of the magnetic field generator to transition from the initial design to the final design that was used in our prototype.

3.4.1. Substitution of some permanent magnet segments by soft magnetic low-carbon steels

Niamjan, N, et al, had simulated a Halbach magnet cylinder consisting of 16 permanent magnet segments. According to their simulation results, they find that the magnetic flux is depleted in some areas (the top and the bottom segments of the magnet cylinder near the edge of the core), so they substituted this Neodymium–Iron–Boron (NdFeB) permanent magnets segments in these areas by soft magnetic low-carbon steel pieces. The introduction of soft magnetic steel reduces the flux density in the air gap but also reduces the cost of the magnet structure[**27**].

3.4.2. Simulation and results:

To reduce our magnet price we decided to reduce the number of the permanent magnet segments, we applied the previous Niamjan study [**27**] to our initial magnet design shown in figure 3.7, which consisted of 16 PM segments. We have designed two different geometries that appear in figure 3.10. Eight magnet segments were replaced by soft magnetic low carbon steel (white), which decreases the price of the magnet by half.

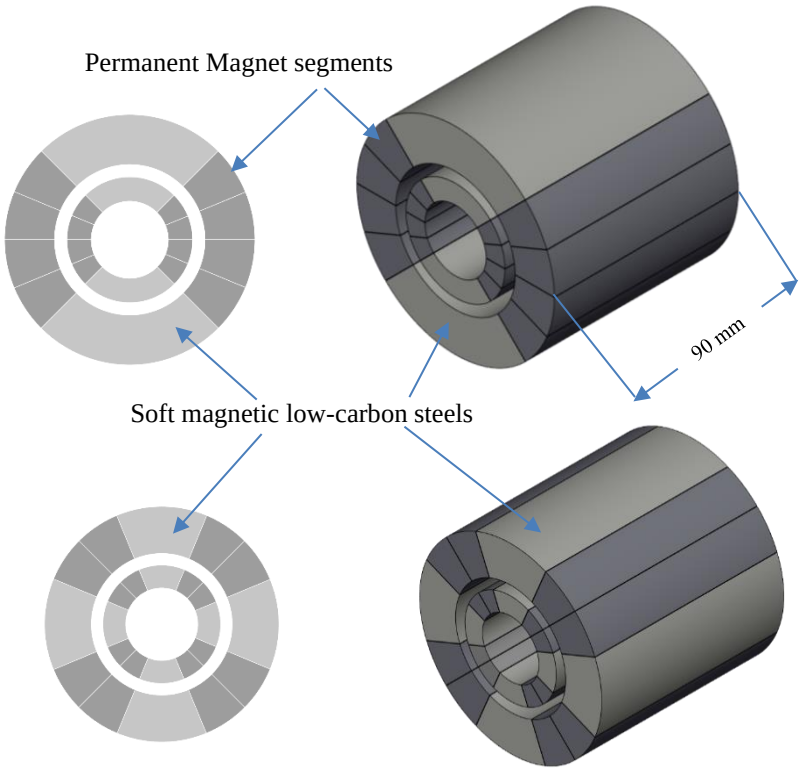

Figure. 3.10: Two different designs of a modified Halbach cylinder composed of adjusted eight permanent magnets and soft magnetic segments.

We perform the two different designs on the Autodesk inventor professional 2021 program, these designs had been simulated by Faraday simulation software, by choosing a point moving in the Y direction at the center of these new designs to measure the magnetic flux density, the simulation results shown in figure 3.11, turns out that the magnetic field has fallen below **1.4 T** (obtained from the initial magnet design), to **0.5 T** obtained from the modified first design and **0.4 T** obtained from the modified second design.

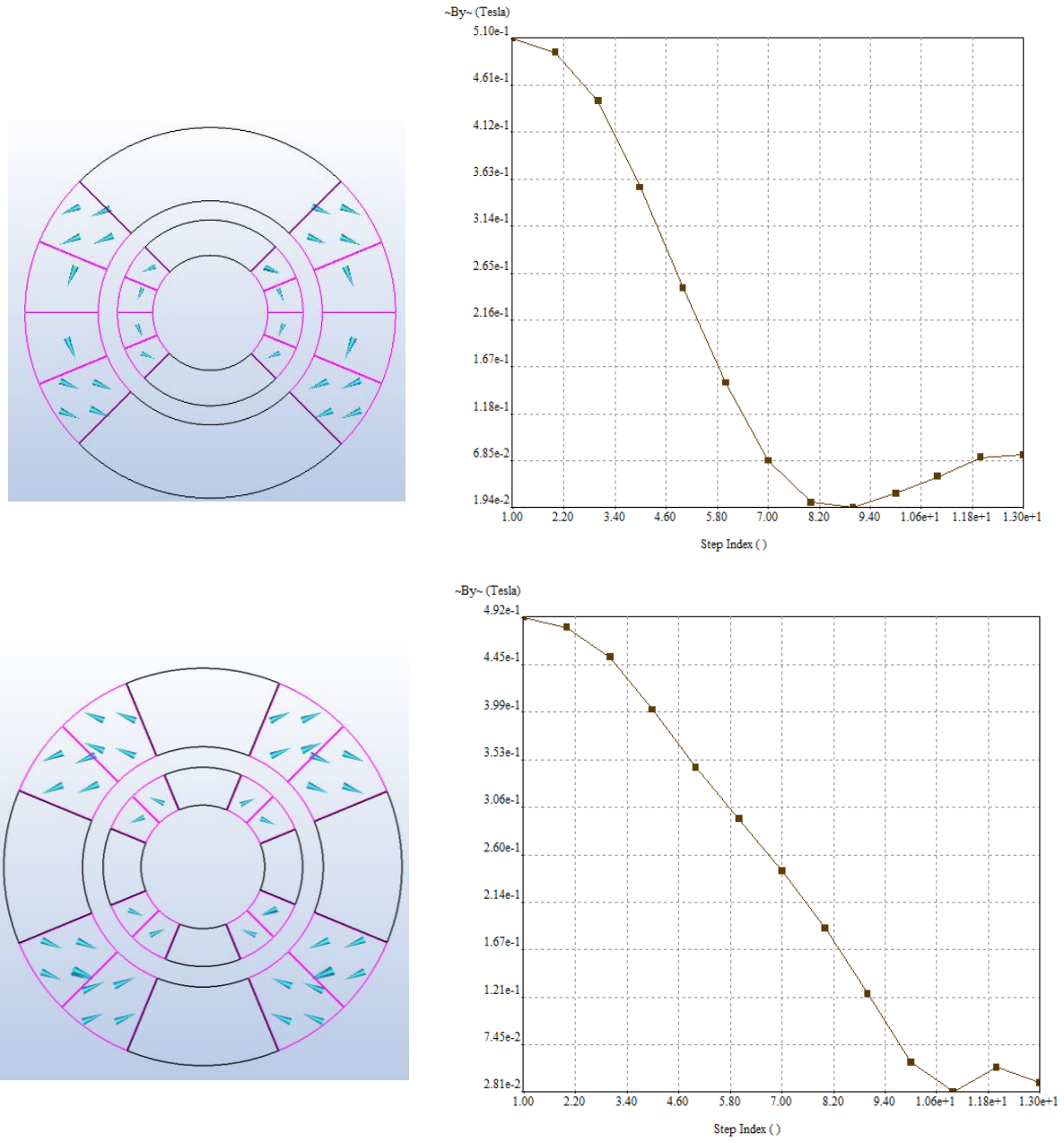

Figure 3.11: Simulating two different designs of a modified Halbach cylinder composed of adjusted eight permanent magnets and soft magnetic segments.

Despite our success in reducing the price of magnets in half by reducing the number of segments, the cost of building magnets is still high, exceeding the budget allocated for this project.

Therefore, we did not apply this study to the magnetic field generator, and we decided to search for another way to reduce the price of building the magnetic field generator.

In the following section, we will show how we have overcome the problem of the high cost of building the magnet.

3.4.3. Transition from ideal Halbach cylinders to discretized cylinders.

Since the price of the magnet remained high despite the reduction of the magnet material, we decided to build the magnet we needed by ourselves, by taking advantage of the presence of manufactured and magnetized ready-made super magnets in different shapes. We kept the dimensions of our initial magnet design shown in black lines in figure 3.12, we choose Super Magnets with dimensions (see figure 3.16) close to the dimensions of the initial magnet cylinders while keeping the length of the cylinder at 90 mm.

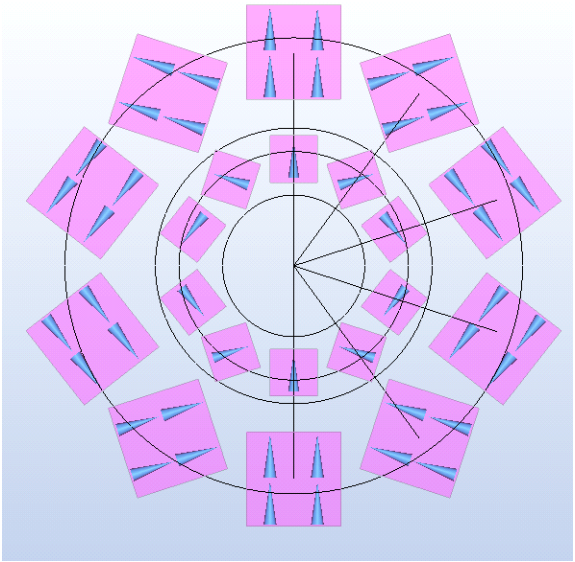

Figure 3.12: A cross-section showing the process of adding the discretized fashion of the magnet to the initial design

The simulation results of this magnet design are shown in figure 3.13.

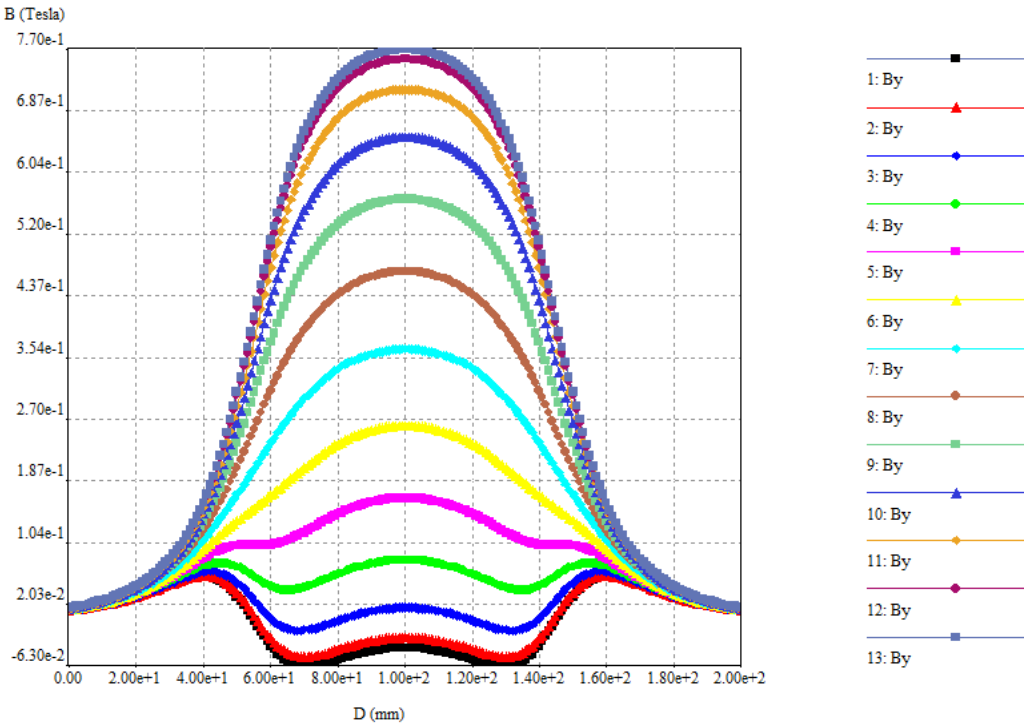

Figure 3.13: The magnetic field along the y axis of the discretized magnet design (0.006 T - 0.7 T), for rotation of the inner magnet cylinder from 0° to 180° (15° every step), the magnet length is 90 mm.

This new design can produce (from **0.0063 T** to **0.77 T**) at the core of the magnet center. According to the rotation of the inner magnet cylinder with respect to the outer one by **15°**, every step appears in different line colors in figure 3.13. But the magnetic field homogeneity needs improvement at the center of the magnet, this point we worked on in the next section.

3.4.4. Improvement of the magnetic field homogeneity

The simulation results in figure 3.14 show the magnetic flux density at the maximum position along with the magnet core for different magnet lengths. The black line represents the magnet flux density along the 90 mm magnet length. The upper orange line represents the magnet flux density along the 180 mm magnet length. It seems clear that linearly increasing the magnet length can improve the magnetic field homogeneity.

But at the same time increasing the length of the magnet does not increase the maximum magnet flux at the center of the magnet. The increase of the length of the magnet from 90 mm – to 180 mm resulted in an increase of just 0.1 T (from 0.7 T produced by 90 mm magnet length to 0.8 T produced by 180 mm magnet length) in the magnetic field.

This result makes us sure that the length of the magnet cylinder does not have a significant impact on the magnetic field density, which was confirmed in equation (3.7).

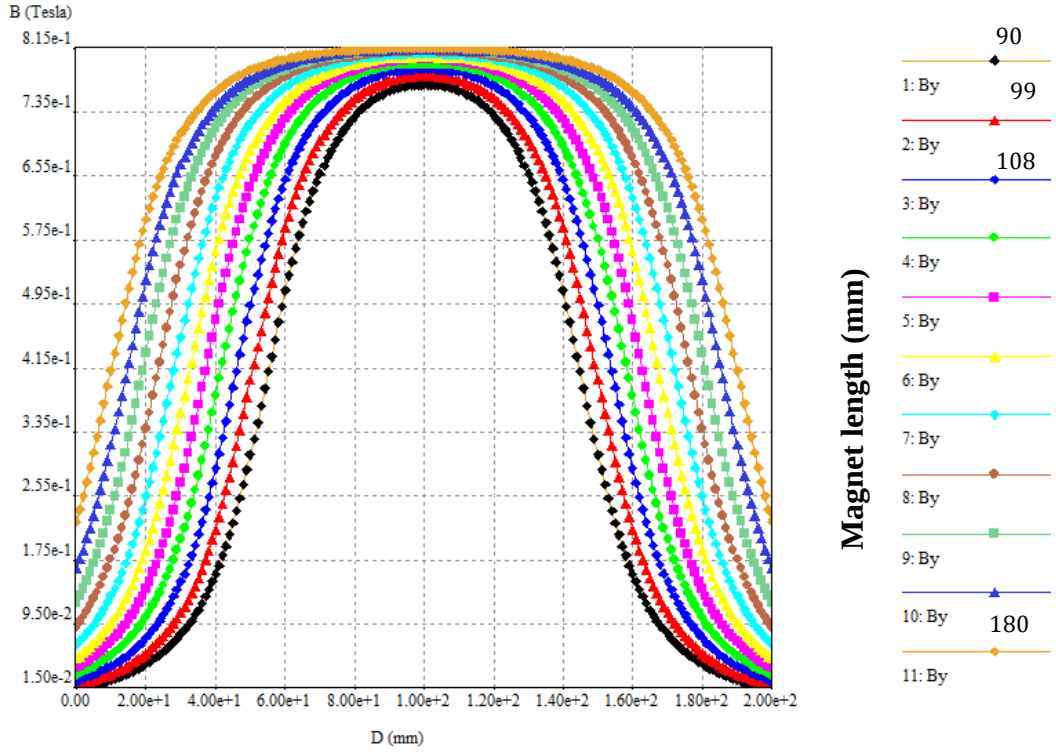

Figure 3.14: Magnetic flux density at the maximum position along the axial direction for different values of magnet lengths (90 mm – 180 mm).

These results encouraged us to improve the magnet and reduce its price by a transition from the expensive nested Halbach initial magnet design (**90 mm** length) to the final magnet design (**180 mm** length), which will be discussed in detail in the next section.

3.5. Magnetic Arrangement for Novel Discrete Halbach Layout (Mandhala)

The Mandhalas were introduced in 2004 as an effective way of providing the homogeneous magnetic field at a low cost since the ideal Halbach cylinders introduced in section 3.3.1 are very expensive. Mandhalas is the discrete version of the ideal one that builds on a single magnet type with one shape and one magnetization direction.

The Mandhalas in figure 3.15 consist of identical cubic bar magnets arranged on a circle, it can produce a magnetic field in the center of the circle. The i^{th} (i = 0, 1,…, n-1) magnet is placed at an angle αi = 2πi/n and its magnetization axis is rotated by βi = 2αi du to the z-axis, with their center vectors, c_{P_i}at an angle α_i on a circle of radius r [36].

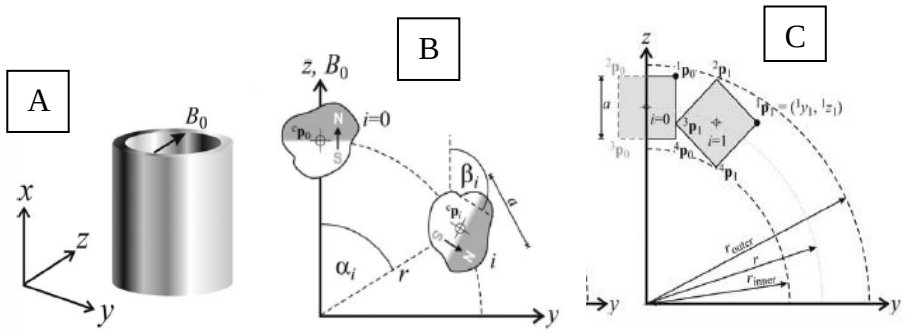

Figure 3.15: Magnetic Arrangement for Novel Discrete Halbach Layout (Mandhala) **(A)** The coordinate system. **(B)** Construction principle of Mandhalas **(C)** Construction using square (cube) magnets [36].

Raich and Blümler [37] indicate that the magnetic field in the center of a Mandhala (B_0) can be calculated by equation (3.7):

$$B_0 = \frac{3.n.(\Xi(n))^3}{\pi}.B_r \qquad (3.7)$$

Where: n is the number of magnets, B_r is the magnet remanence, abbreviation Ξ is a function calculated by [36, 37]:

$$\Xi = \frac{\cos(\frac{2\pi}{n}) - \sin(\frac{2\pi}{n}) - \sqrt{2}.\sin(\frac{\pi}{4} - \frac{4\pi}{n})}{2.\cos(\frac{\pi}{4} - \frac{4\pi}{n}) + \sqrt{2}} \qquad (3.8)$$

Equation 3.8 states that the magnetic field at the center of the Mandhala is determined by the number of magnets (n). Thus, with two concentric magnet cylinders we can have the same magnetic flux density at the center of each Mandhala, this means that we can increase the radius of the mandhala without loss in the field, but the volume of the magnet and the weight will increase, so we should think carefully about the need to increase the radius of the Mandhalas [36].

3.5.1. The final design of the Nested Mandhala magnet cylinders:

The magnetic field source for our magnetocaloric cooling prototype, which had been developed at the Julich Center for Neutron Science (JCNS2) institute is the Nested Mandhala cylinders configuration shown in figure 3.16, which consists of two concentric cylinders, with a length of 180 mm, its length is doubled to increase the magnetic field homogeneity at the magnet core.

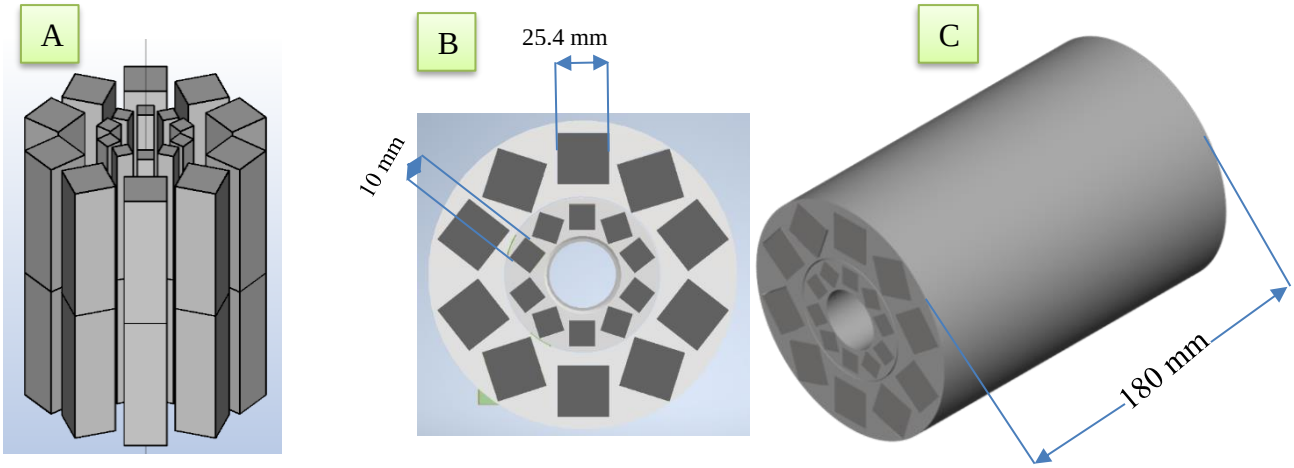

Figure 3.16: Our final nested Mandhala magnet cylinders.

A: The magnet arrays structure B: Cross-section of the magnet C: The magnetic field source.

These magnet arrays are made of cube Neodymium (NdFeB) permanent magnets, its magnet remanence B_r = 1.26-1.32 T (1.3 T average) with dimensions 10 x 10 x 10 mm^3 for the inner rotating cylinder, and cuboid NdFeB magnets, its Remanence B_r = 1.29-1.35 T (1.3 T average) with dimensions 25.4 x 25.4 x 12.7 mm^3 for the outer fixed cylinder shown in Figures 3.17 (A) and (B).

Figure 3.17: Neodymium Super magnets A: Cube magnets (10 x 10 x 10 mm^3), B: Cuboid NdFeB magnet (25.4 x 25.4 x 12.7 mm^3).

The inner Mandhala magnet cylinder consists of 10 columns. Each column consists of 20 cube magnets, each weighing 7.6 g. The outer cylinder consists also of 10 columns, each column consists of 20 cuboid magnets. Each magnet's weight is 62 g.

The magnet flux density (B_O) in the center of the inner Mandhala calculated by using equations (3.7) and (3.8), B_O = 0.3 T. And also 0.3 T for outer Mandhala. Table 3.3 contains a summary of the specifications of our final Mandhala.

Table 3.3: Dimensions and magnitudes of the magnets for the final Mandhala cylinders.

Cylinder	Inner Radius (mm)	Outer Radius (mm)	Each Magnet weight(gm)	Each magnet Dimensions mm^3	Cylinder Volume cm^3	Cylinder length (mm)	Magnet grade	B_r (T)	B_0 (T)
Inner cylinder	30	65	7.6	10 x 10 x 10	4.95	180	N42	1.3	0.3
Outer cylinder	75	160	62	25.4 x 25.4 x 12.7	510.4	180	N40	1.3	0.3

If the magnetic field contributions of each magnet are added as shown in figure 3.18(A) (the inner and outer magnetization in the same direction which means we have 0 degrees between the magnetization direction of the inner magnet arrays and the outer ones), then the maximum magnetic flux density (B_{max}) of the magnet circuit is observed at the core of the inner magnet (see figure 3.19 B) where the magneto-caloric material is located. This process led to

the magnetization of the MCM, which is represented by the red color as a result of its high temperature, the orange arrows represent the remanent flux density orientation of each segment. Conversely, when the magnetic field contributions are subtracted as shown in figure 3.18(B)(the inner and outer magnetization are in opposite directions), then the minimum magnetic flux density ($B_{\min}$)is obtained (shown in figure 3.19 C). It is presented in blue color (see figure 3.18 B) as a result of the low temperature of the refrigerant, due to the demagnetization process.

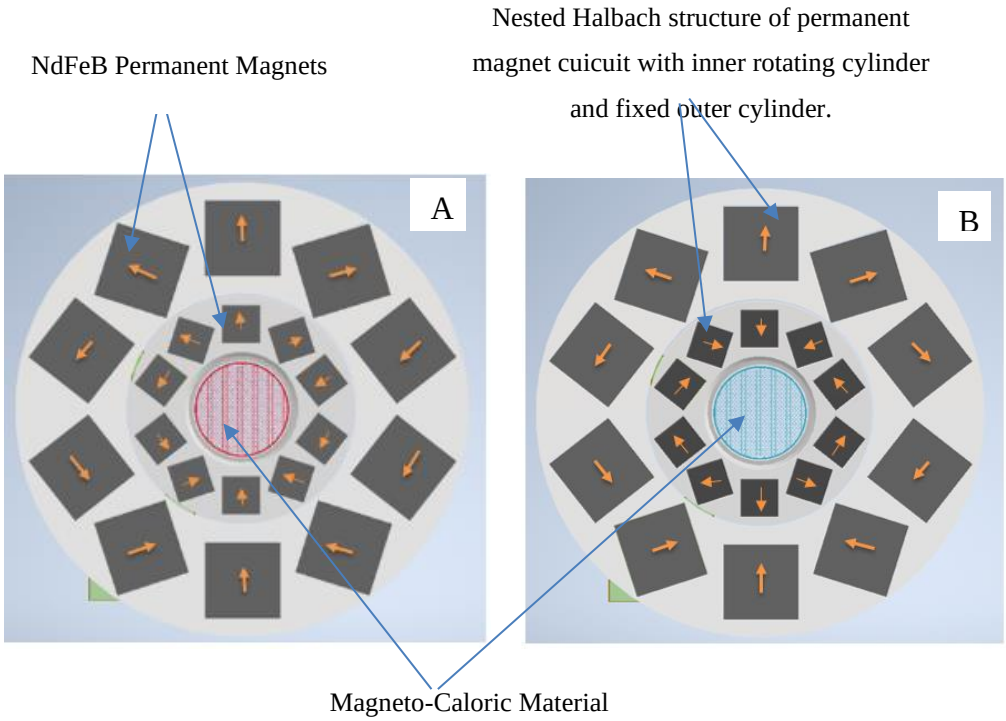

Figure 3.18: The rotary operation principle of magnetic refrigeration Nested Mandhala Halbach structure, **(A):** Magnetization process **(B):** Demagnetization process.

The simulation results for the final nested Mandhala magnet show changes continuously between the maximum flux density (**0.8 T**) and the minimum flux density (**0.001 T**) as shown in figure 3.19, these simulation results are performed by Faraday simulation software.

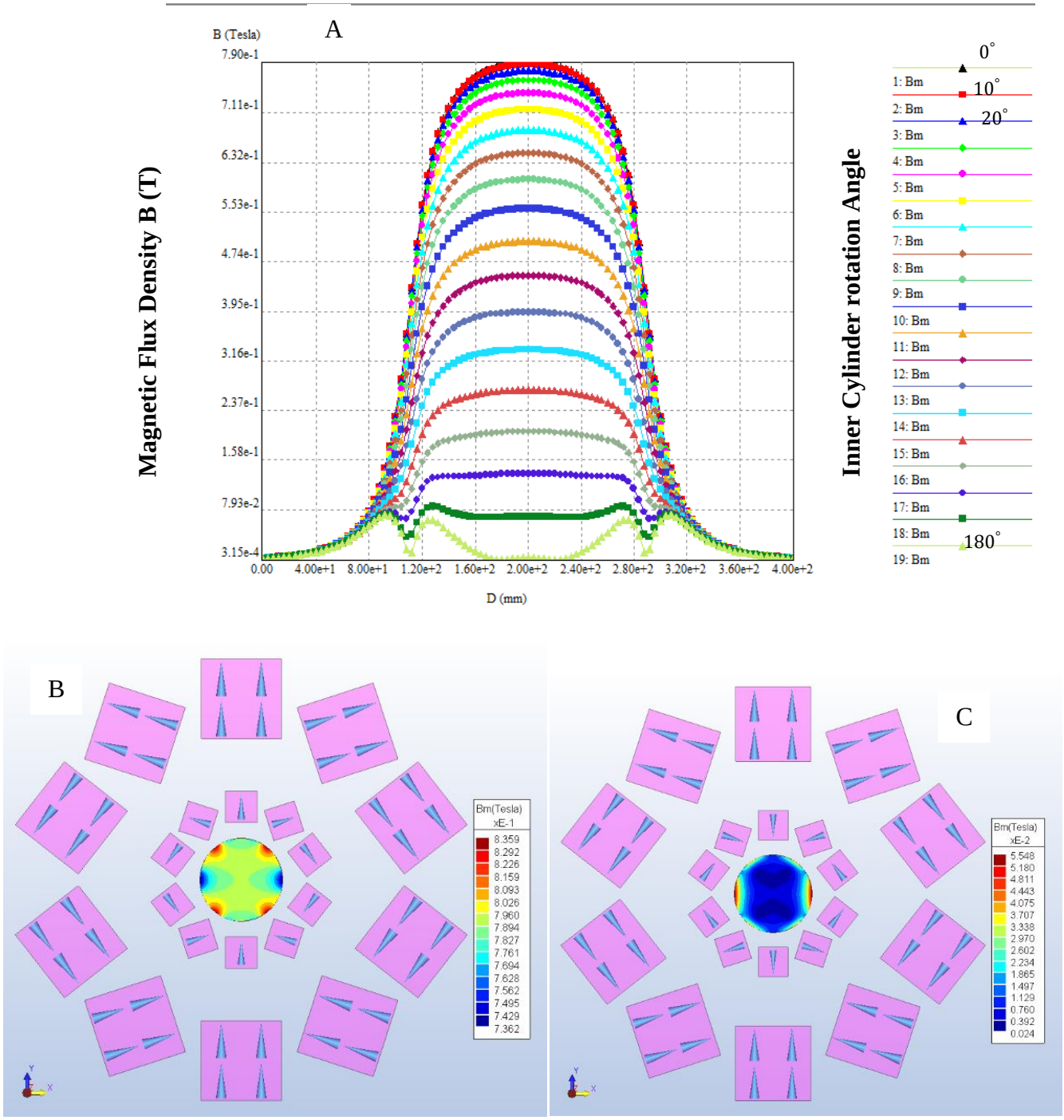

Figure 3.19: The simulation results of our final nested Mandhala magnet cylinders using Faraday software, show the magnetic flux density at the cylinder core. The magnet length is 180 mm.

(A) Magnetic flux density along the axial z-direction for different rotation angles (B): Maximum magnetic flux density (Magnetization) C: Minimum magnetic flux density (Demagnetization).

The different colors of the lines in figure 3.19 A represent the different values of the magnetic field inside the core of the magnet cylinder due to different rotation angles of the inner Mandhala with respect to the outer Mandhala.

Each line represents the rotation of the inner cylinder by 10 degrees, the upper black line represents the **0°** (the maximum magnetic flux density which is also shown in figure 3.19 (B), which equals **0.8 T**). The red line in figure 3.19 (A) represents the magnetic flux density at the magnet core when the inner magnet Mandhala rotates by **20°**. and so on, with continue rotating the inner Mandhala, we reached **180°** represented by the lower green line in figure 3.19 A. this line represents the minimum magnet flux density in figure 3.19 C, which equals **0.001 T**.

3.5.2. Manufacturing Our final Nested Mandhala magnet cylinders:

Figure 3.20 shows the final design of the housing used for the magnet circuit, these designs were performed on the Autodesk inventor program. We have Plates used to fix the magnets and wholes to contain the magnet pieces in order to build our Mandhalas.

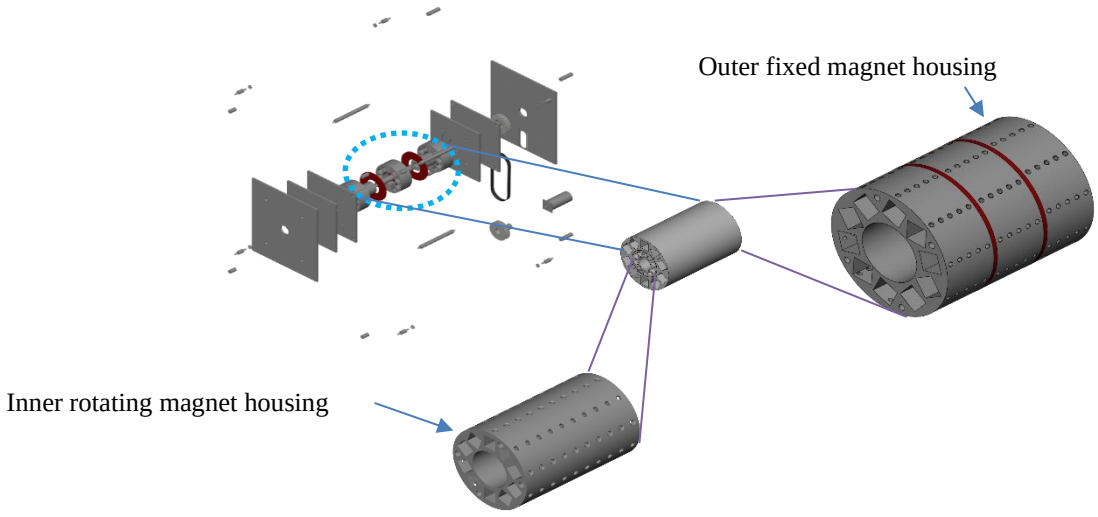

Figure 3.20: The final design of the magnet housing circuit.

The plates are fabricated at the JCNS workshop. And the magnet housings shown in figure 3.21 are made of Polylactide acid (PLA) material produced by a 3D printer at the JCNS2 also.

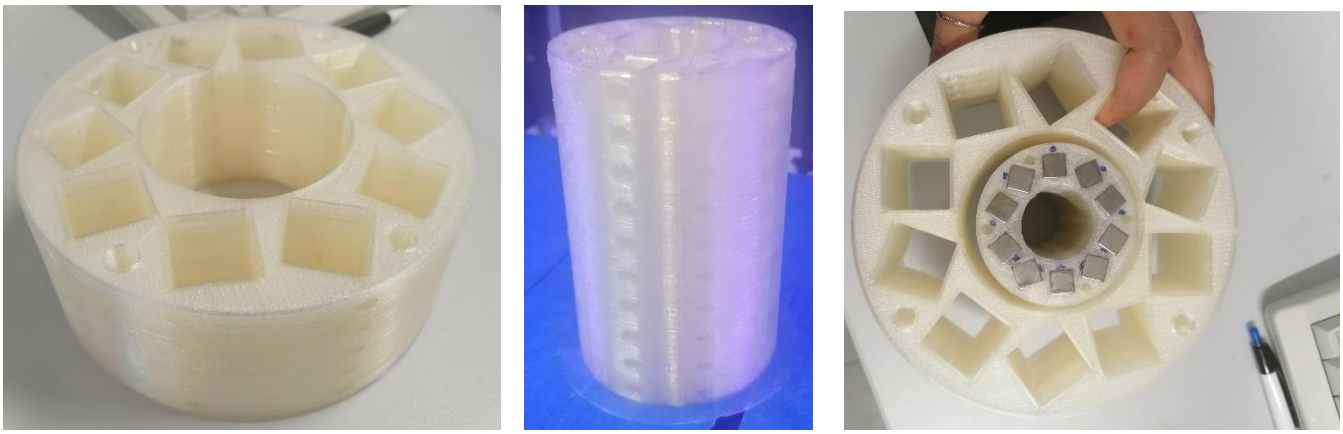

Figure 3.21: 3D printed magnet circuit housing from PLA material.

Figure 3.22 shows the manufacturing of the final design of the magnet circuit (Mandhala) So that we determine the magnetization directions of the magnets using the compass and set their direction on the magnet cover using the marker. After that, the magnet cubes are installed by the pliers using the hammer.

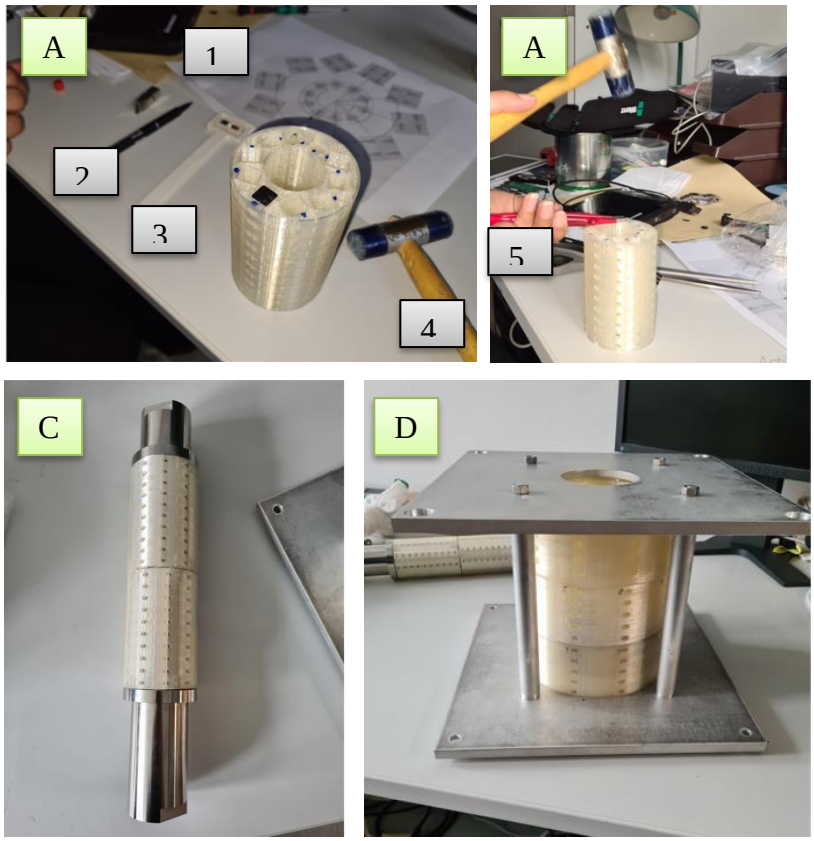

Figure 3.22: Manufacturing Process of our final Mandhala, (A): magnet manufacturing tools, (1): Magnet design, (2): Marker pen, (3): compass, (4): Hammer and (5): pliers, (B): The process of inserting cubic magnets pieces into the Mandhala using the hammer (C): Our Final Manufactured Inner Mandhala cylinder (C): The Final Manufactured Outer Mandhala cylinder.

3.5.3. The magnetic measurement at the center of the internal Mandhala:

We present measurements of the magnetic field generated at the center of our internal Mandhala in figure 3.23 (A), we use an axial Hall probe and transverse fluxmeter for our measurements, shown in figure 3.23 (B). The internal mandhala generated an almost **0.3 T** magnetic field at the center along the x-axis. We observe that any remnant field strengths along the other two axes (y and z) are less than 4% of the maximum attainable field strength along the x-axis, shown in figure 3.23 (B).

Figure 3.23: Measure the magnet flux density inside the inner magnet Mandhala
(A): The inner magnet Mandhala is raised to allow the probe to reach the center of it.
(B): The fluxmeter displays the measured magnetic field inside the inner magnet cylinder.

Table 3.4 represents a comparison between the magnetic field inside the center of the Mandhala, which has been measured practically by fluxmeter, mathematically by equations, and theoretically by simulation results. The results show closeness in the values.

Table 3.4: Results of our nested Halbach magnet cylinders

Results	B_{max}(T)	B_{min}(T)	ΔB (T)
measurements	0.6	**	0.6
Faraday software	0.8	0.001	0.799
Analytical	0.6	0.001	0.599

** B_{min} is not measured, it supposes to be around 0 T.

3.6. Active Magnetic Regenerator (AMR) Design

An AMR consists of a porous matrix of a solid MCM, and an HTF that can flow through the matrix and reject or absorb heat. As we mentioned before in the magnetic refrigeration cycle, it depends on the adiabatic temperature change (ΔT_{ad}) produced by the MCM, this temperature is not big enough for cooling applications, so researchers and scientists utilize a

regenerative process to produce a large enough temperature span to be useful for refrigeration purposes called the active magnetic regeneration (AMR) [**38, 39**].

3.6.1. Active Magnetic Regenerator (AMR)

AMR is a technique that had been used to increase heat exchange, by using a heat-transfer fluid (HTF) in contact with the magnetocaloric materials (MCM), flowing from the cold side to the hot side when the MCM is heated (magnetized), and from the hot side to the cold side when the MCM is cooled down (demagnetized).

This progressively increases the temperature difference between the cold and hot sources, making the system potentially suitable for commercial applications [30], [39].

3.6.2. The type of our Magnetocaloric Material (MCM)

The MCM is the heart of a magnetocaloric cooling device [**38**]. This material needs to have a large adiabatic temperature and entropy change. Also, needs heat conductivity to be as high as possible to efficiently remove the heat generated by the MCE. Furthermore, it needs to be chemically and mechanically stable and shapeable to form a diversity of structures, and cheap. It should have a low rare-earth content, and it needs to be commercially available to be applied in cooling applications widely [**3**].

One of the most promising solid-state refrigerants, which fulfills all of the above conditions is MC alloys with $La(Fe, Si)_{13}$ intermetallic compounds used manganese and hydrogen to adjust the magnetic characteristics of the material [**40, 41**], which was supplied by Vacuumschmelze; a company expert in manufacturing advanced magnetic materials and delivering excellence for over 90 years. This family of MCM products is called Calorivac C [**40**].

3.6.3. The MCM (Calorivac C) properties

Vacuumschmelze describes in figure 3.24 the the isothermal entropy change of the Calorivac C alloys. When these alloyes exposed to different external magnetic fields (0.8 T – 1.5 T).

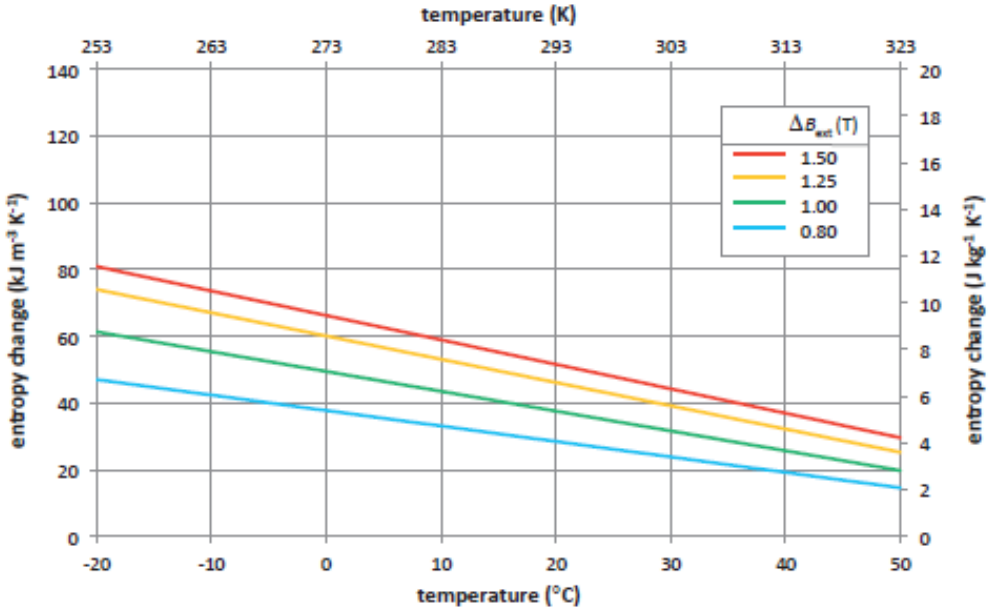

Figure 3.24: Entropy change for Calorivac C alloys for different levels of external magnetic fields (0.8 T – 1.5 T) [40].

And the adiabatic temperature change which shown in figure 3.25, according to exposed Calorivac C alloys to different external magnetic fiels (0.8 T – 1.5 T).

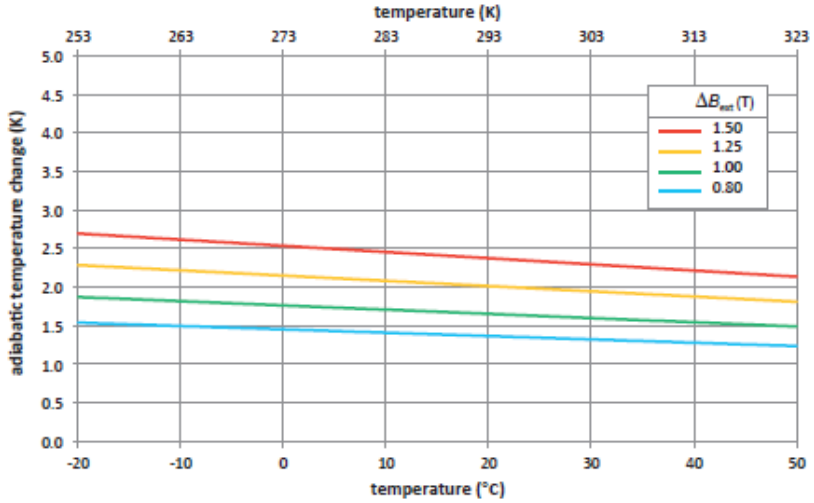

Figure 3.25: Adiabatic temperature change for Calorivac C alloys for different external magnetic fiels (0.8 T – 1.5 T) [40].

Figure 3.26 shows the typical adiabatic temperature change of a series of Calorivac C alloys for an external magnetic induction change of 1.5 T. Calorivac C alloys are available with Curie temperatures over a wide temperature range.

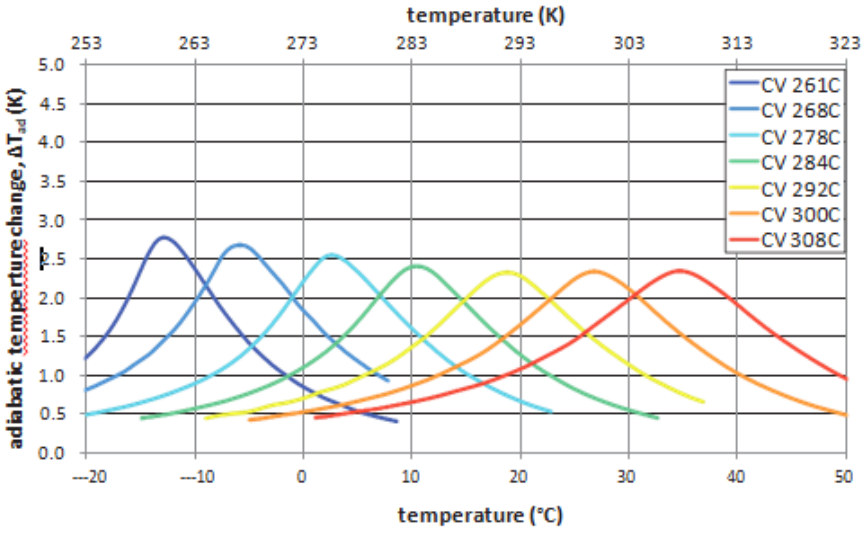

Figure 3.26: Adiabatic temperature change for Calorivac C alloys for a magnetic induction change of 1.5 T [40].

further properties of Calorivac alloys are summarized in table 3.5

Table 3.5: Properties of Calorivac alloys

Thermal conductivity	**6 - 8 $Wm^{-1}K^{-1}$**
Density	7.0 - 7.2 g/cm^3
Relative permeability	800 - 1200

3.6.4. Sample size and geometry

Calorivac alloys can be shaped into various geometries, which makes them the ideal material for complex regenerator designs for magnetocaloric refrigerators. We used a 90 mm cylindrical regenerator shown in figure 3.27 with a diameter of 28 mm consisting of MCM channels equilateral triangles, each edge approximately 30 microns made of La(Fe, $Si)_{13}$ alloys. The HTF passes through these channels to make heat exchange between the MCM and the HTF.

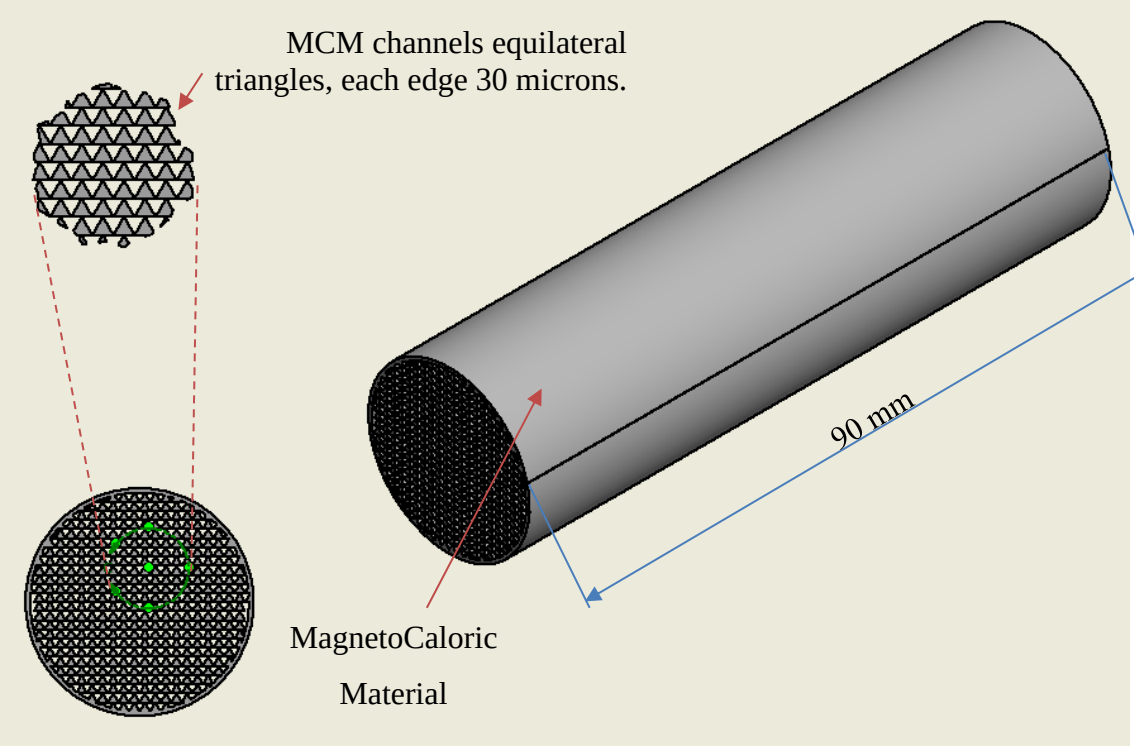

Figure 3.27: Magnetocaloric material geometry.

3.7. Fluid flow/ Heat transfer system

The fluid flow/heat transfer system is responsible for oscillating fluid flow in the magnet regenerator.

Figure 3.28 shows the flowchart of the fluid flow system, which consists of fluid pipes, heat exchangers, pumps, valves, and the fluid reservoir, the components of the fluid flow system is described in detail in Appendix A.

In most cases, water, or aqueous solutions with inhibitors and freezing depressants were used as heat transfer fluid (HTF). Our HTF used in this system consists of 80% water and 20% ethylene glycol. These percentages are used according to literature studies [**21**]. The heat transfer fluid is moved through the regenerator using a pump. The temperatures of the hot reservoir and the cold reservoir are measured by the temperature sensor. The stepper motor is used to limit the length of the magnetization and demagnetization periods by moving the internal magnet cylinder. The motor and the pump are software-controlled by PLC which also controlled the valves according to the periods of the cooling cycle (magnetization period, demagnetization period, hot fluid flow period, and cold fluid flow period).

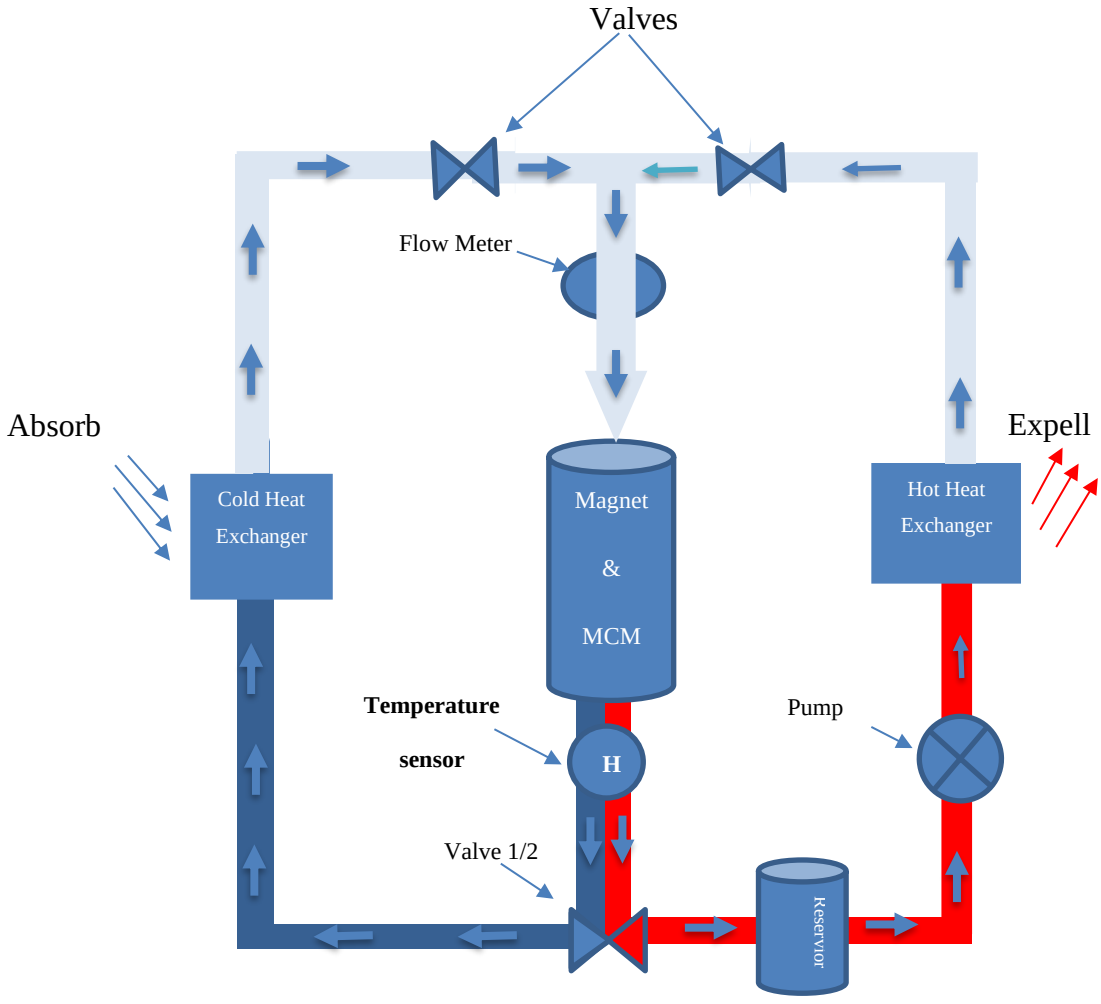

Figure 3.28: Flowchart of the hydraulic system in the magnetic refrigeration system.

3.8. Control system

The flow control system is the part that brings the greatest potential to the whole device, because it is responsible for synchronizing the work of all components, also specifying the timing for every process in the cooling system.

Figure 3.29 shows a schematic diagram illustrating the magnetic refrigeration control system. The components of the control system are described in detail in Appendix B. The central processing unit (S7 – 300) is used to control the state of the valves, according to the blow periods. Also, the pump and motor working are controlled by PLC (S7 – 300) through programming modules (ET 200 S), thus controlling the magnetic field and the flow profile. The operational timing and duration of any valve can be changed by programming the I/O module, which allows comprehensive control of the flow profile of the system.

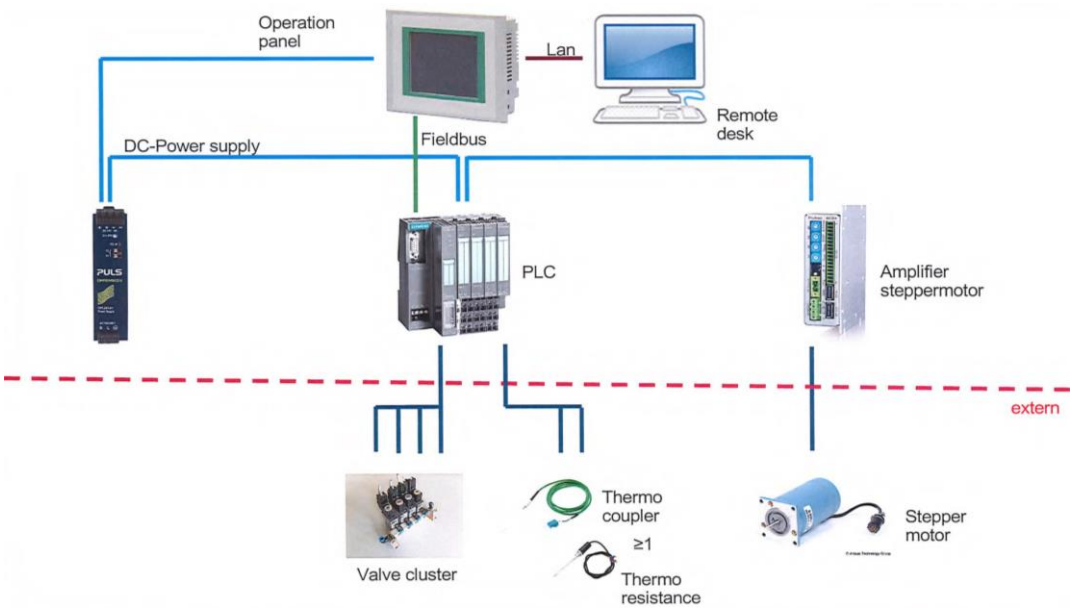

Figure 3.29: A schematic diagram illustrating our magnetic refrigeration control system.

Figure 3.30 presents the control system that we have built.

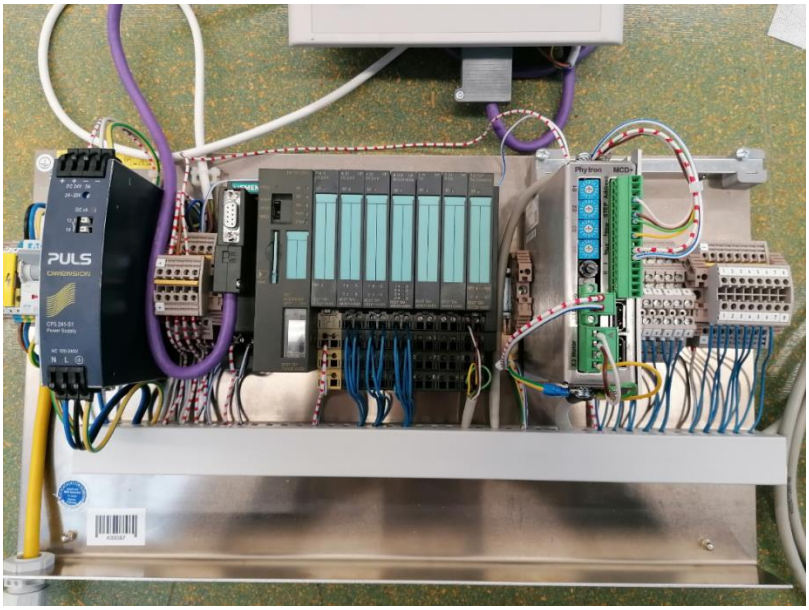

Figure 3.30: Control system of our magneto-caloric cooling device

Chapter 4

4. Conclusions and Future Work

4.1. Conclusions

This thesis presented the development of a sustainable magnetocaloric cooling prototype. An image showing the final magnetic refrigeration model is not provided, due to time constraints.

The greatest effort that has been expended in this thesis is to build and improve the Magnetic Field Generator (MFG), this final MFG is shown in figure 3.22. The MFG is the most expensive part of magnetic cooling prototypes.

According to simulation results, we conclude that :

The initial design of MFG, the two nested Halbach magnet array consisting of two concentric magnet cylinders performed by 16 PM segments and 90 mm magnet length, showed 1.3 T magnetic flux density at the cylinder core using the faraday simulation program, with a very expensive cost.

The final magnet Mandhala design with 180 mm length can produce 0.8 T with a price equivalent to 1/13 of the price of the initial magnet (nested Halbach) which leads us to this conclusion " The MFG has been developed to give us the amount of magnetic field sufficient to cool the magneto-caloric material. The decrease was in this magnetic field equivalent to 36% with a decrease in the price of building the magnetic field generator by 90%. This big drop in the price of magnets is worth this little drop in the amount of magnetic field".

We conclude also, that the length of the magnet does not affect the magnetic field density in the gap of the magnet cylinder. This point leads us to expect the value of the magnetic field resulting from the outer magnet cylinder, which will be approximately equal to the value of the magnetic field in the inner cylinder and equal to approximately 0.3 Tesla, and therefore

the magnet that we have built will give us a maximum magnetic field of approximately 0.6 Tesla.

4.2. Future Work

The first step that must be taken in the future is to simulate the heat transfer between the MCM and the HTF, complete constructing the outer magnet cylinder, and measure the magnetic field intensity inside it(it should be 0.3 T). Then constructing the MFG and also measuring the magnetic field produced (it will be 0.6 T).

Assembling the parts of the four main systems that have been equipped to build and operate our prototype, then evaluating the efficiency, measuring the temperature span, and calculating the cooling power.

In the future, we need to work on the manufacturing of a new magneto-caloric material that can be tested on our device and can be evaluated by comparing the properties of this material with the Calorivac from Vakuumschmelze used in our prototype. Also, we can simulate different geometries for the MCM, and choose the best geometry according to the simulation results.

References

1. B. Huang, J. Lai, D. Zeng, Z. Zheng, B. Harrison, A. Oort, N. van Dijk, and E. Brück, Development of an experimental rotary magnetic refrigerator prototype, International Journal of Refrigeration 104 (2019), 42-50.
2. H. Ucar, D. Paudyal, and O. Boyraz Using numerical methods to screen magnetocaloric materials in an active magnetic regenerative cycle, International Journal of Refrigeration 120 (2020), 50-57.
3. D. Benke, M. Fries, M. Specht, J. Wortmann, M. Pabst, T. Gottschall, I. Radulov, K. Skokov, A. I. Bevan and D. Prosperi, Magnetic refrigeration with recycled permanent magnets and free rare-earth magnetocaloric lafesi, Energy Technology 8 (2020), no. 7, 1901025.
4. D. W. Chun, "Rare-earth free mn-based magnetocaloric alloys for solid-state refrigeration," UC San Diego (2016).
5. R. Kolano, A. Kolano-Burian, M. Hreczka, M. Polak, J. Szynowski, and W. Tomaka, Magnetocaloric cooling device with reciprocating motion of the magnetic field source, Acta Phys Pol A 129 (2016), no. 6, 1205-1209.
6. J. Kaštil, J. Tetek, and A. Tuček, Experimental investigation of small-scale magnetocaloric refrigerator, Acta Physica Polonica, A. 124 (2013), no. 4.
7. D. Eriksen, K. Engelbrecht, C. Bahl and R. Bjørk, Active magnetic regenerator refrigeration with rotary multi-bed technology, PhD Thesis, Technical University of Denmark 2016.
8. N. Mezaal, K. Osintsev and T. Zhirgalova, Review of magnetic refrigeration system as alternative to conventional refrigeration system, IOP Conference Series: Earth and Environmental Science, IOP Publishing, (2017), p. 032024.
9. C. Aprea, A. Greco, A. Maiorino and C. Masselli, Magnetic refrigeration: An eco-friendly technology for the refrigeration at room temperature, Journal of Physics: Conference Series, IOP Publishing, (2015), p. 012026.
10. A. Maiorino, M. G. Del Duca, J. Tušek, U. Tomc, A. Kitanovski and C. Aprea, Evaluating magnetocaloric effect in magnetocaloric materials: A novel approach based on indirect measurements using artificial neural networks, Energies 12 (2019), no. 10, 1871.

11. N. De Oliveira and P. Von Ranke, Theoretical aspects of the magnetocaloric effect, Physics Reports 489 (2010), no. 4-5, 89-159.
12. J. L. Cadena, Designing a rotary magnetic refrigerator, PhD thesis, Federal University of Santa Catarina (2015).
13. A. Tura, Design and analysis of a nested halbach permanent magnet magnetic refrigerator, PhD thesis, University of Victoria (2013).
14. https://www.cibsejournal.com/technical/the-appeal-of-magnetic-refrigeration/.
15. A. Budiman, Modeling of magnetocaloric refrigeration with packed bed regenerator, University of Twente (2016).
16. https://en.wikipedia.org/wiki/Magnetic_refrigeration.
17. K. K. Nielsen and J. H. Hattel, Numerical modeling and analysis of the active magnetic regenerator, Ph.D. Thesis, TDU, Denmark (2010).
18. V. K. Pecharsky and K. A. Gschneidner Jr, Magnetocaloric effect and magnetic refrigeration, Journal of magnetism and magnetic materials 200 (1999), no. 1-3, 44-56.
19. V. Pecharsky, K. Gschneidner Jr, A. Pecharsky and A. Tishin, Thermodynamics of the magnetocaloric effect, Physical review B 64 (2001), no. 14, 144406.
20. A. Kitanovski and P. W. Egolf, Application of magnetic refrigeration and its assessment, Journal of magnetism and magnetic materials 321 (2009), no. 7, 777-781.
21. A. Kitanovski, J. Tušek, U. Tomc, U. Plaznik, M. Ozbolt and A. Poredoš, Magnetocaloric energy conversion, Springer2016.
22. B. Yu, M. Liu, P. W. Egolf, and A. Kitanovski, A review of magnetic refrigerator and heat pump prototypes built before the year 2010, International Journal of refrigeration 33 (2010), no. 6, 1029-1060.
23. A. Kitanovski, J. Tušek, U. Tomc, U. Plaznik, M. Ožbolt, and A. Poredoš, "Overview of existing magnetocaloric prototype devices," Magnetocaloric energy conversion, Springer (2015), pp. 269-330.
24. A. Greco, C. Aprea, A. Maiorino and C. Masselli, A review of the state of the art of solid-state caloric cooling processes at room-temperature before 2019, International Journal of Refrigeration 106 (2019), 66-88.
25. K. Gschneidner Jr and V. Pecharsky, Thirty years of near room temperature magnetic cooling: Where we are today and future prospects, International journal of refrigeration 31 (2008), no. 6, 945-961.

26. D. Benke, J. Wortmann, M. Pabst, T. Gottschall, I. Radulov, K. Skokov, O. Gutfleisch, D. Prosperi, A. Bevan and S. Dove, A green magnetic cooling device built using upcycled NdFeb magnets.
27. N. Niamjan, C. Sirisathitkul, and S. Cheedket, Substitution effect of magnetic materials in Halbach cylinder for magnetic refrigerators, Proceedings of the National Academy of Sciences, India Section A: Physical Sciences (2020), 1-6.
28. J. He, J. Wu, B. Lu, and C. Liu, Comparative study on the series, parallel and cascade cycles of a multi-mode room temperature magnetic refrigeration system, International Journal of Refrigeration (2020).

29. L. M. Maier, P. Corhan, A. Barcza, H. A. Vieyra, C. Vogel, J. D. Koenig, O. Schäfer-Welsen, J. Wöllenstein and K. Bartholomé, Active magnetocaloric heat pipes provide enhanced specific power of caloric refrigeration, Communications Physics 3 (2020), no. 1, 1-6.
30. R. Bjørk, C. R. H. Bahl, A. Smith and N. Pryds, Review and comparison of magnet designs for magnetic refrigeration, International journal of refrigeration 33 (2010), no. 3, 437-448.
31. P. V. Trevizoli, J. A. Lozano, G. F. Peixer and J. R. Barbosa Jr, Design of nested Halbach cylinder arrays for magnetic refrigeration applications, Journal of Magnetism and Magnetic Materials 395 (2015), 109-122.
32. H. R. E.-H. Bouchekara, A. Kedous-Lebouc and J.-P. Yonnet, Design of a new magnetic refrigeration field source running with rotating bar-shaped magnets, International journal of refrigeration 35 (2012), no. 1, 115-121.
33. P. Blümler and F. Casanova, Hardware developments: Halbach magnet arrays, Mobile NMR and MRI: developments and applications 133 (2015).
34. R. Bjørk, C. R. H. Bahl, A. Smith and N. Pryds, Optimization and improvement of Halbach cylinder design, Journal of Applied Physics 104 (2008), no. 1, 013910.

35. J. Hilton and S. McMurry, An adjustable linear Halbach array, Journal of Magnetism and Magnetic Materials 324 (2012), no. 13, 2051-2056.

36. H. Soltner, and P. Blümler, Dipolar Halbach magnet stacks made from identically shaped permanent magnets for magnetic resonance. Concepts Magn. Reson., 36A (2010), 211-222. https://doi.org/10.1002/cmr.a.20165.

37. H. Raich, B. Blümler, Design and construction of a dipolar Halbach array with a homogeneous field from identical bar magnets: NMR Mandhalas. concepts Magn Reson 23B (2004), 16-25. https://www.blogs.uni-mainz.de/fb08-physics-halbach-magnets/files/2017/12/NMR-Mandhalas.pdf.

38. A. Kitanovski, Energy applications of magnetocaloric materials, Advanced Energy Materials 10 (2020), no. 10, 1903741.

39. R. Bjørk, A. Smith, C. R. H. Bahl, and N. Pryds, Determining the minimum mass and cost of a magnetic refrigerator, International journal of refrigeration 34 (2011), no. 8, 1805-1816.

40. H. VACUUMSCHMELZE GmbH & Co. KG, "Magnetocaloric materials calorivac," vol. 2021, Shanghai Sales Office, Room 06, 19F, Zhongrong Hengrui International Plaza, 2015.

41. M. Krautz, K. Skokov, T. Gottschall, C. S. Teixeira, A. Waske, J. Liu, L. Schultz, and O. Gutfleisch, Systematic investigation of mn substituted lafe si alloys and their hydrides for room-temperature magnetocaloric application, Journal of Alloys and Compounds 598 (2014), 27-32.

"تطوير نموذج أولي لجهاز تبريد مغناطيسي مستدام"

اعداد : فاطمة بطاط

الملخص

التبريد المغناطيسي (MR) هي تقنية تبريد جديدة تستخدم المبردات الصلبة بدلاً من المبردات الغازية المستخدمة في تقنيات التبريد التقليدية. المبرد الصلب هو مادة مغناطيسية (MCM) ، عندما تتعرض المادة المغناطيسية لمجال مغناطيسي خارجي فانها تزداد حرارتها، وبالتالي عند ازالة المجال المغناطيسي الخارجي تقل درجة حرارة المادة المغناطيسية. تسمى الظاهرة التي تصف تغير درجة حرارة المادة المغناطيسية والتي تعتبر أساس تقنيات التبريد المغناطيسي بالتأثير المغناطيسي (MCE). بالمقارنة مع دورة ضغط البخار التقليدية ، فإن دورة التبريد المغناطيسية أكثر كفاءة في استخدام الطاقة وأكثر صداقة للبيئة لأنها لا تستخدم غازات الدفيئة.

في هذه الأطروحة ، قمنا بتطوير نموذج أولي لجهاز تبريد مغناطيسي مستدام. من خلال اجراء دراسة شاملة لنماذج التبريد المغناطيسي التي تم بناؤها قبل العام 2020 وتم الاتفاق على الشكل الاولي والمواصفات الاولية للنموذج المنوي بناؤه. تم اختيار التصميم المناسب للنموذج الأولي وتم تنفيذه على برنامج Autodesk inventor 2021 .

تم اختيار مكونات نموذج التبريد المغناطيسي الخاص بنا وتقسيمها إلى أربعة أقسام رئيسية على النحو التالي: مولد المجال المغناطيسي (MFG) يتكون من المغناطيس والية عمله) ، المجدد المغناطيسي النشط (AMR) الذي يحوي المادة المغناطيسية ، نظام تدفق السوائل / نقل الحرارة، و نظام التحكم.

تم الاتفاق على المكونات الرئيسية لهذه الانظمة والبدء بجمعها لبناء النموذج. بما ان مولد المجال المغناطيسي هو اغلى جزء في نموذجنا الاولي فقد تم بذل كل الجهد لتحسينه وتطويره وخفض سعره الذي فاق ميزانيتنا.

تم اختيار مولد مجال مغناطيسي (هالباخ)، الذي يتكون من اسطوانتين متداخلتين، داخلية متحركة وخارجية ثابتة، مثبت في وسط الاسطوانة الداخلية حامل سنقوم بتثبيت المادة المغناطيسية بداخله، ونتيجة لدوران الاسطوانة الداخلية بالنسبة للخارجية يتم توليد مجالين مغناطيسيين مسلطين على المادة المغناطيسية، مما يؤدي لتغير درجة حرارتها مولدا فرق بالحرارة يتم استغلاله في عملية التبريد.

تم تنفيذ تصميمات مختلفة لمولد المجال المغناطيسي MFG على برنامج Autodesk inventor وتمت محاكاتها على برنامج Faraday ، كان التصميم الاولي عبارة عن مغناطيس هالباخ يتكون من اسطوانتين متداخلتين بطول 90 مم تتكونان من قطع مغناطيسية صغيرة وكثيرة، يستخدم مغناطيس هالباخ لتوليد مجال مغناطيسي في مكان معين والغائه في الاماكن الاخرى، استطاع هذا النموذج انتاج مجال مغناطيسي كثافته 1.4 تسلا في مركز الاسطوانة الداخلية حيث يتم تثبيت المادة المغناطيسية هناك، ولكن في نفس الوقت كان سعرهذا التصميم غاليا جدا.

الجهد الاكبر الذي تم بذله في رسالة الماجستير هذه انصب على تصميم مولد مجال مغناطيسي MFG بسعر قليل. قمنا بعمل تصميمات اخرى تحوي قطع مغناطيسية اقل بمقدار النصف عن النموذج الاول ، وقمنا بعمل محاكاة لهذه التصاميم بحيث اظهرت نتائج المحاكاة ان التصميم الجديد يمكنه توليد مجال مغناطيسي كثافته 0,5 تسلا وبالتالي تم خفض سعر المغناطيس الى النصف، ولكن للاسف بقي سعره غاليا جدا ونحن محكومون بميزانية اقل بكثير من سعر المغناطيس.

في التصميم النهائي قمنا باستبدال مغناطيس هالباخ Halbach المثالي بـ الـ Mandhalas، وهو عبارة عن مغناطيس هالباخ ولكن يتم بناؤه من قطع مغناطيس مصنعة وجاهزة تباع باشكال اسطوانية او مكعبات او متوازي مستطيلات، قمنا بتصميم جديد للمغناطيس المتكون من هذه المغناطيسات جاهزة الصنع وبعد عمل محاكاة لتصميمنا النهائي استطعنا الحصول على مجال مغناطيسي يعادل 0.8 تسلا اي ما يعادل نقص في المجال المغناطيسي الذي حصلنا عليه بنسبة 36%، ولكن الشيء الجميل الذي حصل معنا اننا خفضنا سعر المغناطيس بنسبة 90 %، هذا النزول الكبير بالسعر يجعلنا نغض اطرف عن النزول القليل في المجال المغناطيسي.

في التصميم النهائي قمنا باستبدال مغناطيس هالباخ

تم تصنيع مصفوفة Mandhala المتداخلة المحسَّنة نتيجة لنتائج المحاكاة. تم التحقق من صحة تصميم مصفوفة Mandhala Halbach المُحسَّنة ومقارنتها. تم التأكيد على أن مصفوفة Halbach المُحسَّنة أكثر فاعلية لنموذج MR الأولي الخاص بنا من مصفوفة Halbach المغناطيسية المتداخلة الأولية.

قمنا ببناء هذا المغناطيس الاخير بعد ان صممنا هيكل داعم له على برنامج اوتودسك انفنتور، وقمنا بطباعته على طابعة 3D في معهد يوليش لعلوم النيوترون، قمنا بشراء قطع المغناطيس مكعبة الشكل ومتوازية مستطيلات، وقمنا ببناء المغناطيس النهائي. قمنا بقياس المجال المغناطيسي في مركز الاسطوانة الداخلية للمغناطيس النهائي بوساطة جهاز قياس التدفق المغناطيسي فوجدنا ان النتيجة قريبة جدا من نتيجة عملية محاكاة المغناطيس.

قمنا بمضاعفة طول اسطوانة المغناطيس (من 90 مم الى 180 مم) مما زاد الهوموجينتي داخل الاسطوانة، وكانت الزيادة في المجال بسيطة جدا.

تم اختيار AMR عن طريق اختيار نوع وهندسة MCM المستخدمة لوضعها في أسطوانة المغناطيس الداخلية قمنا بشراء المادة المغناطيسية من شركة Vacuumschmelze والتي تسمى مادة Calorivac.

تم تخطيط نظام التحكم ويعتمد على المكونات الفردية التي يمكن الوصول إليها بسهولة والمتاحة بالفعل في معهد يولش للابحاث. تم أيضًا تصميم نظام تدفق السوائل / نقل الحرارة وكما تم شراء المكونات.

Appendix A

Fluid flow/ Heat transfer system

The components of the Fluid flow/ Heat transfer system are:

1. **The hot heat exchanger (Alphacool Radiator 95 euro):** This radiator's performance in expelling heat is high because all the main elements the fins, the channels, and the antechambers are made of copper.

Figure 1: Alphacool full copper radiator.

2. **Temperature sensor TM4101: (Pt100 70 euro):**

   Our temperature sensor shown in figure 3, warranting precise temperature measurement in containers, tanks, and pipelines can be connected to an evaluation unit. It has a very short response time for use in processes with rapid temperature changes, robust stainless steel housing with a high degree of protection and high-pressure resistance.

Figure 2: Temperature sensor.

3. **Alpha cool pump (VPP655 – single (78 euro))**: used for circulation of the heat transfer fluid.

Figure 3: The pump

4. Fan (NB – Black Silent Pro):

The fan is shown in figure 4.22 with dimensions, of 140 x 140 x 25 mm^3, it minimizes the transmission of vibrations. The frame was designed for use on radiators, where in addition to decoupling, it ensures optimal sealing. This prevents air from escaping through the minimal gap between the fan and radiator and thus contributes to cooling. It features an auto-restart function, very low noise, and a very high life expectancy of 140,000 hours.

Figure 4: The hot heat exchanger fan.

5. **Reservoir** (62 euro): The fluid reservoir is used to hold a volume of heat transfer fluid of the system.

Figure 5: Reservoir

Valves: Vesto solenoid Valve (24 V DC) shown in the next figure, are responsible for controlling the direction and timing of the heat transfer fluid flowing in the vessels.

Figure 6: Vesto solenoid Valve

Pipes: blue plastic tubing with 12 mm diameter from Festo company, used to transfer HTF from one part to another in the cooling system.

Figure 7: Pipe

Appendix B

Flow control system:

The flow control system is the part that brings the greatest potential to the whole device, because it's responsible for synchronizing the work of all components, also specifying the timing for every process in the cooling system.

Control System:

The components of the control system are:

1. **Power Supply** (Puls CP5.241-S1 (136 euro)): power supply with AC input range (100 – 240 V AC), and output voltage DC 24V, with easy fuse breaking, used to provide power for the motor, and valves to switch on/off. Also, we used (12 V DC) used to provide power for the pumps and the fan.

Figure 1: Power Supply from PULS Company (24 V DC).

2. **Monitor (Touch Screen 6AV6642-0BA01-1AX1 Siemens (1200 euro))**: used to display graphs for fluid pressure, flow rate, magnetization /demagnetization periods, and the temperature at heat exchangers

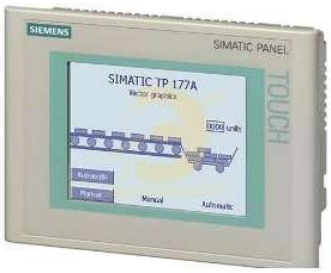

Figure 2: Monitor touch screen from Siemens

3. **Central Processing Unit PLC** (CPU SIMATIC S7-300 (Price 965 euro))

Central processing unit needs 24 V DC power supply, with work memory 128 KB, used to control and synchronizing the system.

Figure 3: Central processing unit (PLC)

4. **Customized IO system for compact control cabinets – (SIMATIC ET 200 S):**
   It is consists of digital input and output modules (DI), analog input and output modules (Al), base units (D0), and a motor stepper, which used to control the On/OFF valves, stepper motor motion, On/Off pump to have a complete cooling cycle.

Figure 4: I/O system for compact control cabinets with IO modules and base unit.

5. **Step Motor** (SLO-SYN DC motor)**:**

This SLO-SYN DC motor shown in figure 7 is used to rotate the inner cylinder of the magnet to produce magnetization and demagnetization processes.

Figure 5: stepper motor

6. **Voltage Amplifier:** The purpose of an amplifier in a motion control system is to provide a controlled amount of voltage to a motor based on a command signal from the motion controller. This is done by a voltage amplifier.